DCDC2 Mutations Cause a Renal-Hepatic Ciliopathy by Disrupting Wnt Signaling

Markus Schueler,[1,20] Daniela A. Braun,[1,20] Gayathri Chandrasekar,[2,20] Heon Yung Gee,[1,20] Timothy D. Klasson,[3] Jan Halbritter,[1] Andrea Bieder,[2] Jonathan D. Porath,[1] Rannar Airik,[1] Weibin Zhou,[4] Joseph J. LoTurco,[5] Alicia Che,[5] Edgar A. Otto,[4] Detlef Böckenhauer,[6] Neil J. Sebire,[7] Tomas Honzik,[8] Peter C. Harris,[9] Sarah J. Koon,[9] Meral Gunay-Aygun,[10] Sophie Saunier,[11] Klaus Zerres,[12] Nadina Ortiz Bruechle,[12] Joost P.H. Drenth,[13] Laurence Pelletier,[14,15] Isabel Tapia-Páez,[2] Richard P. Lifton,[16,17] Rachel H. Giles,[3] Juha Kere,[2,18,19,*] and Friedhelm Hildebrandt[1,17,*]

Nephronophthisis-related ciliopathies (NPHP-RC) are recessive diseases characterized by renal dysplasia or degeneration. We here identify mutations of *DCDC2* as causing a renal-hepatic ciliopathy. DCDC2 localizes to the ciliary axoneme and to mitotic spindle fibers in a cell-cycle-dependent manner. Knockdown of *Dcdc2* in IMCD3 cells disrupts ciliogenesis, which is rescued by wild-type (WT) human *DCDC2*, but not by constructs that reflect human mutations. We show that DCDC2 interacts with DVL and *DCDC2* overexpression inhibits β-catenin-dependent Wnt signaling in an effect additive to Wnt inhibitors. Mutations detected in human NPHP-RC lack these effects. A Wnt inhibitor likewise restores ciliogenesis in 3D IMCD3 cultures, emphasizing the importance of Wnt signaling for renal tubulogenesis. Knockdown of *dcdc2* in zebrafish recapitulates NPHP-RC phenotypes, including renal cysts and hydrocephalus, which is rescued by a Wnt inhibitor and by WT, but not by mutant, *DCDC2*. We thus demonstrate a central role of Wnt signaling in the pathogenesis of NPHP-RC, suggesting an avenue for potential treatment of NPHP-RC.

Introduction

Cilia are microtubule-based structures that project from the cell surface of numerous mammalian cells and mediate key pathways of development such as Wnt and Shh signaling. Many ciliary proteins participate in functional protein subcomplexes,[1] which localize to primary cilia, centrosomes, the mitotic spindle, or the abscission structure in a cell-cycle-dependent manner.[2] Mutations in genes that encode these ciliary proteins lead to developmental and degenerative diseases, which show a broad phenotypic spectrum. This complex of disorders has collectively been termed "ciliopathies" due to their localization to primary cilia and centrosomes.[3] Moreover, numerous cilia-mediated signaling pathways have been implicated in the pathogenesis of ciliopathies, such as canonical Wnt/β-catenin,[4] Shh,[5] and DNA damage response (DDR).[6,7]

In this context, the term nephronophthisis-related ciliopathies (NPHP-RC) summarizes a group of rare autosomal-recessive cystic kidney diseases including nephronophthisis (NPHP [MIM 256100]), Senior-Loken syndrome (SLS [MIM 266900]), Joubert syndrome (JBTS [MIM 213300]), and Meckel Gruber syndrome (MKS [MIM 249000]). NPHP accounts for the majority of genetically caused end-stage renal disease (ESRD) during the first three decades of life. The most prominent diagnostic hallmarks are increased echogenicity and the presence of corticomedullary cysts upon renal ultrasound. Histologically, NPHP is characterized by tubular atrophy, basement membrane disintegration, interstitial fibrosis, and cyst formation. About 15% of the affected individuals with NPHP-RC exhibit extrarenal organ involvement, in particular hepatobiliary ductal plate malformation, progressive retinal dystrophy, and cerebellar vermis hypoplasia/aplasia as the hallmark of JBTS. The most severe manifestation of the NPHP-RC spectrum is MKS, a perinatally lethal ciliopathy.

Similar to the vast pleiotropy, NPHP-RC show broadly heterogeneous genotypes with monogenic ciliopathies established to be caused by recessive mutations in more

[1]Department of Medicine, Boston Children's Hospital, Harvard Medical School, Boston, MA 02115, USA; [2]Department of Biosciences and Nutrition, Karolinska Institutet, 14183 Huddinge, Sweden; [3]Department of Nephrology and Hypertension, University Medical Center Utrecht, 3584CX Utrecht, the Netherlands; [4]Department of Pediatrics and Communicable Diseases, University of Michigan, Ann Arbor, MI 48109, USA; [5]Department of Physiology and Neurobiology, University of Connecticut, Storrs, CT 06269, USA; [6]University College London, Institute of Child Health and Pediatric Nephrology, Great Ormond Street Hospital, London WC1N3JH, UK; [7]Department of Histopathology, Great Ormond Street Hospital, London WC1N3JH, UK; [8]Department of Pediatrics and Adolescent Medicine, First Faculty of Medicine, Charles University and General University Hospital, Ke Karlovu 2, Prague 2, 128 08 Czech Republic; [9]Division of Nephrology and Hypertension, Mayo Clinic, Rochester, MN 55905, USA; [10]Medical Genetics Branch, National Human Genome Research Institute, National Institutes of Health, Bethesda, MD 20892, USA; [11]Inserm U574 and Department of Genetics, Paris 5 University, Necker Hospital, 75015 Paris, France; [12]Institute of Human Genetics, University Hospital, RWTH Aachen, 52074 Aachen, Germany; [13]Department of Gastroenterology and Hepatology, Radboud UMC, P.O. Box 9101, 6500 HB Nijmegen, the Netherlands; [14]Lunenfeld-Tanenbaum Research Institute, Mount Sinai Hospital, 600 University Avenue, Toronto, Ontario M5G 1X5, Canada; [15]Department of Molecular Genetics, University of Toronto, Toronto, Ontario M5S 1A8, Canada; [16]Department of Genetics, Yale University School of Medicine, New Haven, CT 06510, USA; [17]Howard Hughes Medical Institute, Chevy Chase, MD 20815, USA; [18]Molecular Neurology Research Program, University of Helsinki, and Folkhälsan Institute of Genetics, 00014 Helsinki, Finland; [19]Science for Life Laboratory, Karolinska Institutet, 171 21 Solna, Sweden
[20]These authors contributed equally to this work
*Correspondence: juha.kere@ki.se (J.K.), friedhelm.hildebrandt@childrens.harvard.edu (F.H.)
http://dx.doi.org/10.1016/j.ajhg.2014.12.002.

than 90 genes.[3–5,8–15] We recently demonstrated in a large cohort of 1,056 families with NPHP-RC that in more than 50% of cases the underlying disease-causing mutation is unknown.[16,17] In order to identify additional single gene causes of NHPH-RC, we here applied homozygosity mapping and whole-exome sequencing in 100 affected individuals of consanguineous parents or sibling cases fulfilling the diagnostic criteria of NPHP-RC. In combination with high-throughput exon sequencing in a cohort of 800 individuals with NPHP-RC, we identified recessive truncating mutations in *DCDC2* as a hitherto unknown cause of renal-hepatic variant of NPHP-RC. We demonstrate that DCDC2 interacts with the mediator of Wnt signaling dishevelled, and that *DCDC2* overexpression inhibits β-catenin-dependent Wnt signaling. Thus, we demonstrate a central role of Wnt signaling in the pathogenesis of NPHP-RC, suggesting an avenue for potential treatment of NPHP-RC.

Material and Methods

Research Subjects

Blood samples and pedigrees were obtained from individuals with diagnosed NPHP-RC and informed consent. Approval for human subject research was obtained from Institutional Review Boards of the University of Michigan and the Boston Children's Hospital.

Linkage Analysis

For genome-wide homozygosity mapping GeneChip® Human Mapping 250k StyI Array (Affymetrix) was used. Regions of homozygosity were identified using GENEHUNTER 2.1[18,19] and ALLEGRO[20] with a disease allele frequency of 0.0001 and marker allele frequencies of European descent.[12,21]

Whole-Exome Sequencing

Whole exome sequencing (WES) and variant burden analysis was performed as previously described[22] using Agilent SureSelect human exome capture arrays (Life Technologies™) with next generation sequencing (NGS) on an Illumina™ sequencing platform. Sequence reads were mapped against the human reference genome (NCBI build 36/hg18) using CLC Genomics Workbench (version 4.7.2) software (CLC bio). Mutation calling (Tables S1 and S2) was performed by geneticists/cell biologists, who had knowledge of clinical phenotypes, pedigree structure, homozygosity mapping, and WES evaluation.

High-Throughput Mutation Analysis by Array-Based Multiplex PCR and NGS

For 48 DNA samples simultaneously, 672 amplicons (592 exons) of 32 candidate genes, including *DCDC2*, were sequenced in a cohort of 800 individuals with NPHP-RC using a PCR-based 48.48 Access Array microfluidic technology (Fluidigm) with consecutive NGS as previously described.[16,17] Detected variants were confirmed by Sanger sequencing and evaluated for segregation. Additional 21 individuals with early onset liver fibrosis were Sanger sequenced for coding regions of *DCDC2* (Table S3).

cDNA and Splice Mutation

RNA of A4435-21 and healthy control was purified from whole blood, cDNA was synthesized (Agilent Technologies) and Sanger sequenced, using primers flanking exon 4 in order to confirm skipping of exon 4 (Figure S1; Table S3).

cDNA Cloning

Human full-length (Hs-FL) *DCDC2* cDNA was subcloned by PCR from Hs-FL cDNA (origene SC114336). Full-length and partial clones were subcloned into pRK5-N-Myc using the gateway system (Invitrogen). Mutations were introduced at position c.649A>T to represent p.Lys217* (Figure S2C) and at c.123_124 delGT to represent p.Ser42Glnfs*72 (Figure S2A) using "QuikChange II XL Site-Directed Mutagenesis" (Agilent Technologies). Using the same technique the nucleotides 349 to 425 of exon 4 were deleted in order to represent the splice mutation c.349-2A>G (Figure S2B). *MAPK8IP1* (*JIP1*) full-length was subcloned from Hs-FL cDNA (NM_005456, origen sc124125) into pDEST40 (gateway). *PAFAH1B1* (*LIS1*) (NM_000430.3 [MIM 601545]), open reading frame was amplified from Hs-FL cDNA (clone ID HsCD00378475) and subcloned to pDEST40. Human *Dishevelled 1,2,3* (NM_004421.2, NM_004422.2, NM_004423.3) full-length clones and fragment of *DVL3* were a gift from Vita Bryja, Masaryk University.

Coimmunoprecipitation

Coimmunoprecipitation experiments upon co-overexpression in NIH 3T3 and HEK293T cells were performed as described previously.[23]

Luciferase Reporter Gene Assay

The Wnt/β-catenin reporter assay has been performed as described.[23] In brief, NIH 3T3 cells were transfected with pcDNA3/S33Y β-catenin, pTOPFLASH, pGL4.74[hRluc/TK] (Promega) and *DCDC2* (WT/mutants) or the empty vectors. At 36 hr posttransfection, luciferase activities were measured using a Dual-Luciferase® Reporter Assay and GloMax™ 96 microplate luminometer (Promega) according manufacturer's instruction. The luciferase activities were normalized to Renilla luciferase activities and protein concentration.

Antibodies

For immunofluorescence studies, the following primary antibodies were used: Mouse anti-DCDC2 (Abcam, ab 157186), goat-anti-DCDC2 (Santa Cruz, sc-50728), rabbit anti-Kif3a (Abcam ab11259), mouse anti-Jip-1 (Santa Cruz sc-25267), mouse anti-DVL3 (Santa Cruz sc-365581), mouse anti-SDCCAG8 (Abcam, ab67098), rabbit anti-Cep164 (Sigma, hpa037606), mouse anti-Pericentrin (Abcam, ab28144), rabbit anti-PCNT (Atlas Antibodies, 019887), rabbit anti-PCM-1 (Cell Signaling, 5259), and rabbit anti-IFT88 (ProteinTech, 13967-1-AP). For immunoblotting, the following primary antibodies were used: rabbit anti-DCDC2 (Sigma Aldrich D2945), and mouse anti-Jip-1 (Santa Cruz sc-25267).

Immunofluorescence and Confocal Microscopy in Cell Lines

Cells were prepared for immunofluorescence as previously described[24], incubated in primary antibodies (see above) overnight at 4°C, and imaged using Leica SP5X system with an upright DM6000 microscope and A1R confocal microscope (Nikon Instruments).

Immunofluorescence and Confocal Microscopy on Tissues

Human and murine paraffin-embedded samples were obtained from Zyagen. Paraffin-embedded tissue sections of 5–7 μm were deparaffinized, rehydrated, stained after heat-induced antigen retrieval, and imaged on a LSM510 confocal microscope (Carl Zeiss Microimaging), and on an A1R confocal microscope (Nikon Instruments).

Knockdown of *Dcdc2*

Transfection of non-target siRNA was performed in parallel to targeted siRNA using Lipofectamine RNAimax (Invitrogen) following manufacturer's instructions. Experiments were performed 48 hr after siRNA transfection. For all knockdown experiments, Dharmacon ON-TARGETplus siRNA 11 and 12 against murine *Dcdc2a* were used (Table S3). The knockdown efficiency was shown by immunoblot (Figure S12) and by qPCR (Figure S10).

Spheroid Assay

Spheroid assays were performed as previously described.[6] In brief, IMCD3 cells were transfected with human *DCDC2* cDNA constructs at day 1. After 24 hr, cells were transfected with siRNA against murine *Dcdc2a*. 24 hr after the second transfection, cells were resuspended in matrigel (BD Bioscience) and seeded on Lab TekII chambered coverglasses. After 72 hr, cells that had formed spheroids with visible cleared lumens were stained and imaged using a Zeiss LSM700 confocal microscope. In each spheroid, nuclei were counted, followed by cilia. The percentage of "ciliated nuclei" in each spheroid was used as a distinct value in the results. To detect the presence of cilia, we scored 200–2,000 cells per condition for the presence of cilia. GraphPad Prism 6.0 (GraphPad Software) was used to graph results and perform statistical tests using ANOVA statistical analysis. Experiments were repeated at least two times independently and data combined, graphs show mean value and SEM.

Zebrafish Embryos and Microinjections of Morpholinos and mRNA

Zebrafish embryos were staged 24 hr post fertilization (hpf) and 1-phenyl-2-thiourea (PTU, Sigma) was used to block pigmentation in embryos older than 24 hpf. A morpholinooligonucleotide (MO) against the translation start site of *dcdc2b* (AUGMO) (Table S3) was designed (Gene Tools, LLC), dissolved in 1× Danieau's buffer and injected at varying concentrations (50, 100, 150, 200, and 250 μM) into WT zebrafish embryos at the one-cell stage. 5′-capped sense mRNA of human *DCDC2* WT and the two mutant clones *hDCDC2_Lys217** and *hDCDC2_Ser42Glnfs*72* were synthesized using SP6 mMessage mMachine Kit (Ambion) and was coinjected (approximately 100 pg) with *dcdc2b* MO for rescue experiments. Two additional MOs targeting splice sites were not efficient in *dcdc2b* knockdown as evidenced by RT PCR (data not shown). All zebrafish experiments were performed in accordance with ethical permits approved by Stockholm North Experimental Animal Committee (Dnr N29-12).

Treatment with WNT/β-Catenin Inhibitor iCRT14

Zebrafish embryos injected with AUGMO were exposed to 500 nM or 750 nM or 1 μM or 5 μM concentrations of iCRT14 at the beginning of gastrulation. Compound treated embryos were raised at 28.5°C in Petri dishes for 48 hr and screened for the rescue of ciliopathy phenotypes. As solvent control, 1% DMSO was used.

Whole-Mount In Situ Hybridization, Histology, and Immunohistochemistry

Digoxigenin-labeled antisense probe for *foxa3* was synthesized as described previously.[25] For in situ hybridization staged embryos were fixed in 4% PFA for 24 hr and processed.[26] Immunohistochemistry and histology experiments on Zebrafish embryos have been performed as described.[27,28]

Transmission Electron Microscopy

For electron microscopy, 3.5-day-old control and morphant embryos were fixed in 2% glutaraldehyde solution containing 1% PFA in 0.1 M phosphate buffer (PB), pH 7.4. Sectioning was performed using a Leica EM UC 6 (Leica) and stained with uranyl acetate and lead citrate. Electron micrographs were examined and acquired using a Tecnai 10 transmission electron microscope with a veleta camera.

Statistical Analysis

Results in Figure 2 are presented as scattergrams with means and error bars for SD for the indicated number of values. Statistical analysis of continuous data was performed with a two-tailed Student's t test. $p < 0.05$ was considered statistically significant.

Bioinformatics

Genetic location is according to the February 2009 Human Genome Browser data.

Results

DCDC2 Mutations Cause a Renal-Hepatic Ciliopathy

To elucidate pathomechanisms of NPHP-RC, we sought additional causative mutations and performed homozygosity mapping[21] and whole-exome sequencing[24] in 100 consanguineous cases or sibling cases fulfilling the diagnostic criteria of NPHP-RC. In consanguineous individual A3547-22, who had hepatic fibrosis (Figure 1A) at age 11 months and end-stage renal disease (ESRD) from NPHP at age 14 years (Table 1), we obtained by homozygosity mapping eight candidate regions of homozygosity by descent (Figure 1B). Whole-exome sequencing yielded a homozygous truncating mutation (c.649A>T, p.Lys217*) in *DCDC2* (double cortin domain-containing 2) (Figures 1C–1E; Table 1). No additional homozygous truncating mutations were detected in any other gene within the mapped candidate regions (Tables S1 and S2). Direct inspection of sequence alignments did not yield a mutation in any of the >90 genes with a known connection to NPHP-RC. By high-throughput exon sequencing[16,17] in a large worldwide cohort of 800 additional families with NPHP-RC, in whom mutations in known genes were excluded, we sequenced all exons of *DCDC2*. In less than ten of these individuals liver fibrosis was present. We detected in individual A4435-21, who had hepatic fibrosis requiring liver transplantation at 2 years of age, two compound heterozygous mutations: A frameshift mutation (c.123_124 delGT, p.Ser42Glnfs*72) (Table 1; Figure 1E) and an obligatory splice site mutation (c.349-2A>G) that we show produces the frameshift product p.Val117Leufs*

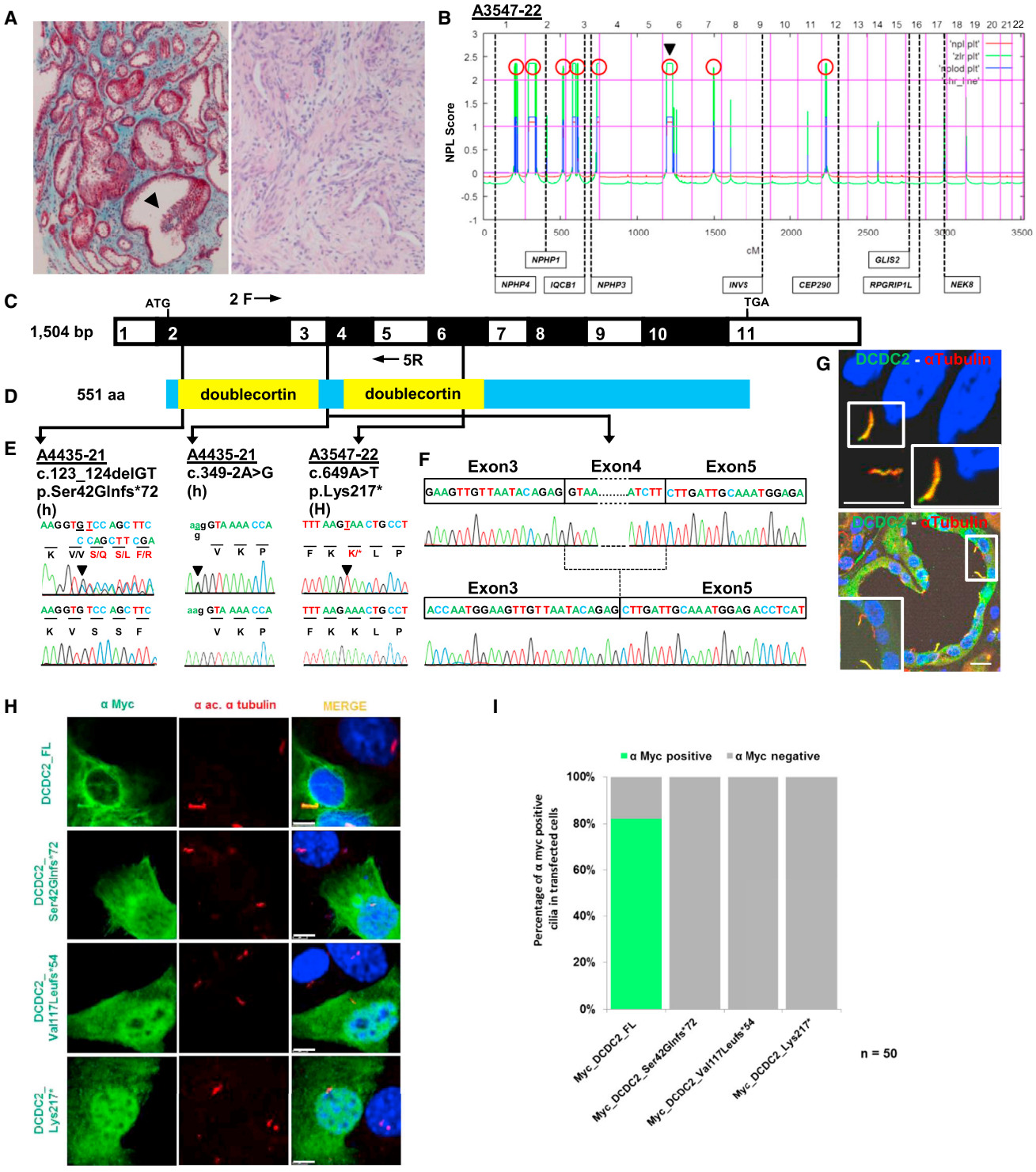

Figure 1. Homozygosity Mapping and WES Detect *DCDC2* Mutations in Individuals with Renal-Hepatic Ciliopathy

(A) In A3547-22 with a renal-hepatic ciliopathy renal histology (left panel; Masson trichrome staining) reveals tubulointerstitial fibrosis and tubular dilation with epithelial luminal budding (arrowhead). Hepatic histology (right panel; H&E staining) of A3547-22 shows areas of florid fibrosis with destruction of bile ducts, focal ductular proliferation with cholestasis, and bile plugging.

(B) For individual A3547-22 nonparametric LOD (NPL) scores from whole-genome mapping are plotted across the human genome. The x axis shows Affymetrix 250K *Sty*I array SNP positions on human chromosomes concatenated from pter (left) to qter (right). Genetic distance is given in cM. Eight maximum NPL peaks (red circles) indicate candidate regions of homozygosity by descent. Note that the *DCDC2* locus (arrow head) is positioned within a maximum NPL peaks on chromosome 6p.

(C) Exon structure of human *DCDC2* cDNA. Positions of start codon (ATG) and stop codon (TGA) are indicated.

(D) Protein domain structure of DCDC2. The N terminus contains two doublecortin domains.

(legend continued on next page)

54 (Table 1; Figure 1F; Figures S1 and S2). None of the affected individuals had retinal degeneration, cerebellar vermis hypoplasia, hydrocephalus, obesity, or bone disease. An additional 21 individuals with early onset liver fibrosis were screened for variants in the coding region of *DCDC2* by Sanger sequencing (Table S3). No additional mutations were detected. We generated cDNA clones reflecting the human *DCDC2* mutations (Figure S2). When re-evaluating the *Dcdc2* knockout mouse model,[29] we found that there was periportal fibrosis at age 11 months consistent with the phenotype seen in humans with *DCDC2* mutations (Figure S3).

DCDC2 Colocalizes with Other NPHP-RC Proteins to the Cilia-Centrosome-Spindle Complex

To elucidate the role of DCDC2 in the pathogenesis of NPHP-RC, we examined its localization in epithelia of different tissues that are involved in NPHP-RC phenotypes, using indirect immunofluorescence studies. In kidney and liver, we observed that DCDC2 colocalizes with acetylated α-tubulin to the axoneme of primary cilia of human renal tubule cells and cholangiocytes in liver (Figure 1G) and to multiciliated ependymal cells and pia mater cells in mouse brain (Figure S4). However, DCDC2 did not localize to the basal body (Figure S4).

Because NPHP-RC proteins localize to primary cilia, centrosomes, the mitotic spindle, and the abscission structure in a cell-cycle-dependent manner,[2] we performed colocalization studies for DCDC2 and other NPHP-RC proteins using confocal laser immunofluorescence microscopy in MDCK-II and hTERT-RPE1 cells (Figures S6 and S7). We found that within the different phases of mitosis DCDC2 fully or partially colocalizes with acetylated α-tubulin during metaphase and anaphase to the spindle microtubules, during late telophase/diakinesis to the abscission structure, and in ciliated cells during interphase to the ciliary axoneme (Figures S5–S7). Throughout those cell-cycle phases, DCDC2 is excluded from the basal body (in interphase) and the mitotic spindle poles (in metaphase and anaphase), as well as the midbody (in diakinesis) (Figures S5–S7), in contrast to other NPHP-RC proteins, which preferentially stain basal body and spindle poles, reciprocally omitting the axoneme and mitotic spindle fibers. These NPHP-RC proteins include SDCCAG8/NPHP10 (Figure S6) and CEP164/NPHP15 (Figure S7). In metaphase, DCDC2 is absent from the interpolar spindle domain of the mitotic spindle (Figure S5). Three proteins that had been described as interacting with DCDC2, DVL3 (this study), JIP1,[30] and Kif3a[31] labeled basal bodies, mitotic spindle poles, and midbody rather than the ciliary axoneme (Figure S8).

Overexpression in hTERT-RPE1 cells revealed upon immunofluorescence that mutations observed in individuals with NPHP-RC and constructs, from which either of the two doublecortin domains are deleted (Figure S2) fail to localize to the primary cilia (Figure S9). These results are in accordance to observations made in rat hippocampal neurons.[31] Immunocytochemistry of cells overexpressing WT and the truncating mutants p.Lys217*, p.Val117Leufs*54, and p.Ser42Glnfs*72 shows that the mutations abrogate localization of DCDC2 to the primary cilium in NIH 3T3 (Figure 1H) and RPE1 cells (Figure S9).

DCDC2 Interacts with DVL1-3, and Mutations Abrogate Wnt Signaling

Because we have previously shown that INVS[4,32] and CEP164,[6] defects in which are associated with NPHP-RC, interact with proteins that participate in Wnt signaling, we tested whether DCDC2 interacts with the disheveled proteins (DVL1, DVL2, or DVL3), which act as regulators of Wnt signaling.[31,33]

We performed coimmunoprecipitation studies in NIH 3T3 cells demonstrating that full-length DCDC2 interacts with all three dishevelled proteins, DVL1, DVL2, and DVL3. This interaction was not abrogated in cDNA constructs representing the mutations that we identified in individuals with NPHP-RC (Figure S11). However, a construct (aa 222-476) lacking both doublecortin (DCX) domains (see Figure S2) failed to interact with DVL3, whereas deletion of either DCX domain alone did not abrogate interaction with DVL3 (Figure 2A). (An overview on cDNA clones is given in Figure S2, where p.Ser42Glnfs*72 represents the shortest variant of A4435-21).

As DVL regulates Wnt signaling, we examined signaling effects downstream of DCDC2 and found that siRNA knockdown of *Dcdc2a* in NIH 3T3 cells increases β-catenin-induced activation of T cell factor (TCF)-dependent transcription (Figure 2B). Reciprocally, overexpression of *DCDC2* WT reduced β-catenin-induced activation of TCF-dependent transcription (Figure 2C, left panel). This effect was abrogated by all three mutations (Table 1, Figures 1C–1E) that we detected in individuals with

(E) Three homozygous (H) or compound-heterozygous (h) *DCDC2* mutations detected in two families with a renal-hepatic ciliopathy (see Table 1). Family number (underlined), mutation, and predicted translational changes are indicated. Healthy control sequence is shown underneath.
(F) Sequenced RT-PCR product from cDNA of lymphocytes of A4435-21 with obligatory splice mutation (c.349-2A>G) using primers located in exons 2 (2F) and 5 (5R). Positions of primers are indicated in (C).
(G) Hepatic and renal localization of DCDC2. Coimmunofluorescence using anti-DCDC2 or anti-α-acetylated tubulin antibodies demonstrates DCDC2 at the ciliary axoneme in cilia of cholangiocytes (upper panel) and of renal epithelial cells (lower panel). Immunofluorescence was performed on human paraffin embedded sections. Nuclei are stained with DRAQ5. Scale bars are 20 μm.
(H) Upon overexpression in NIH 3T3 cells WT DCDC2 decorates the ciliary axoneme, whereas all three mutant clones reflecting mutations in NPHP-RC families lack ciliary localization.
(I) Quantitation of ciliary staining in 50 transfected cells per clone. Scale bars are 5 μM.

Table 1. Mutations of *DCDC2* in Two Families with Nephronophthisis-Related Ciliopathies

Family-Individual	Ethnic Origin	Nucleotide Alteration[a] (Segregation)	Deduced protein Change	Exon/intron (state)	Parental Consanguinity	Kidney Phenotype	Liver Phenotype	Other (Clinical Characteristics)
A3547–22	UK	c.649A>T (M: het, P: het)	p.Lys217*	6 (Hom)	Yes	Increased echogenicity, severe interstitial fibrosis, tubular dilation with prominent epithelial luminal budding, ESRD at 14 yr. died at 16 yr. from esophageal bleeding	Hepatosplenomegaly, extensive florid fibrosis with destruction of bile ducts, bile focal duct proliferation with cholestasis	Left terminal ICA region aneurysm, foci of signal abnormality in subcortical and deep white matter
A4435–21	Czech	c.123_124 delGT (M: het) c.349-2A>G (P: het)	p.Ser42Glnfs*72[b] 3′ splice site (100% conserved) (p.Val117Leufs*54)[c]	2 (het) 4 (het)	No	No renal involvement current age 9 yr.	Hepatosplenomegaly, ductal plate malformation, hepatic fibrosis, scant cholestasis, LTX at 2 yr.	N/A

CRF, chronic renal failure; ESRD, end-stage renal disease; het, heterozygous; Hom, homozygous; ICA, internal carotid artery; LTX, liver transplantation; M, maternal; N/A, not applicable; P, paternal; yr., years.
[a]*DCDC2:* cDNA mutations are numbered according to human cDNA reference sequence NM_001195610.1.
[b]The allele appears 12/8,242 in the EVS-Server database.
[c]G is not among alternative nucleotides in the splice site consensus (3′ acceptor splice site position). The allele appears 3/67366 in the ExAC Browser database.

NPHP-RC (Figure 2C, left panel). Two different Wnt inhibitors (FH535 and iCRT14) reduced β-catenin-induced activation of TCF-dependent transcription with an effect that was additive when combined with *DCDC2* overexpression (Figure 2C, middle and right panels).

DCDC2 Interacts with JIP1

Previous studies showed that DCDC2 interacts with the protein JIP1 (mitogen-activated protein kinase 8 interacting protein 1).[30,34] JIP1 plays a role in aggregating components of the MAP kinase module (MLK, MKK7, JNK), in facilitating JNK signal transduction[35] activating JNK,[36] thereby mediating MAPK activation. We therefore performed coimmunoprecipitation in HEK293T cells (Figure S12A). Whereas WT DCDC2 and the mutant p.Val117Leufs*54 still interacted with full-length JIP1, the DCDC2 truncated mutant p.Ser42Glnfs*72 that we had detected in individual A4435-21 lacked interaction with JIP1. (For DCDC2 constructs see Figure S2.) When phosphorylation of the JNK downstream targets c-Jun and ATF2 was assayed in NIH 3T3 cells, knockdown of *DCDC2* in NIH 3T3 cells did not affect JNK pathway activation (Figure S12B). It was previously shown that lissencephaly-1 (LIS1) interacts with doublecortin (DCX), a protein that belongs with DCDC2 to a family of doublecortin domain-containing proteins.[37] When performing coimmunoprecipitation to test for interaction of DCDC2 with LIS1 we did not detect an interaction between the two proteins (Figure S13).

Loss of Dcdc2 Function Disturbs Renal Epithelial Ciliation in 3D Cultures

In order to test the effects of DCDC2 on ciliation, we assessed the result of *Dcdc2* siRNA knockdown in a 3D cell culture system. IMCD3 cells cultured in 3D matrigel mimic the normal processes of renal tubulogenesis by forming spheroids or small tubules composed of polarized cells, which exhibit a lumen and a ciliated apical membrane. Counting the number of cilia present on this apical membrane is an established model of ciliogenesis.[38] Spheroids grown from cells treated with two different RNAi oligonucleotides targeted against *Dcdc2* displayed significantly fewer cilia than spheroids grown from cells treated with a non-target control RNAi but did not display any severe architectural changes in lumen formation (Figure 3). In both cases, this ciliation defect could be rescued by concurrent transfection of WT human *DCDC2* but not by any of the mutant *DCDC2* clones Ser42Glnfs*72 and Val117Leufs*54 that were derived from the affected individuals (Figures 3A–3C). The third mutant (Lys217*) was not efficiently expressed in the spheroids. The overexpression of empty vector, human WT *DCDC2*, or either of the mutants did not produce a significant difference in ciliation, excluding a dominant-negative or overexpression effect caused by these alleles (Figure 3; Figure S10). We conclude that DCDC2 is important for the generation and maintenance of renal cilia, but knockdown of *DCDC2* does not

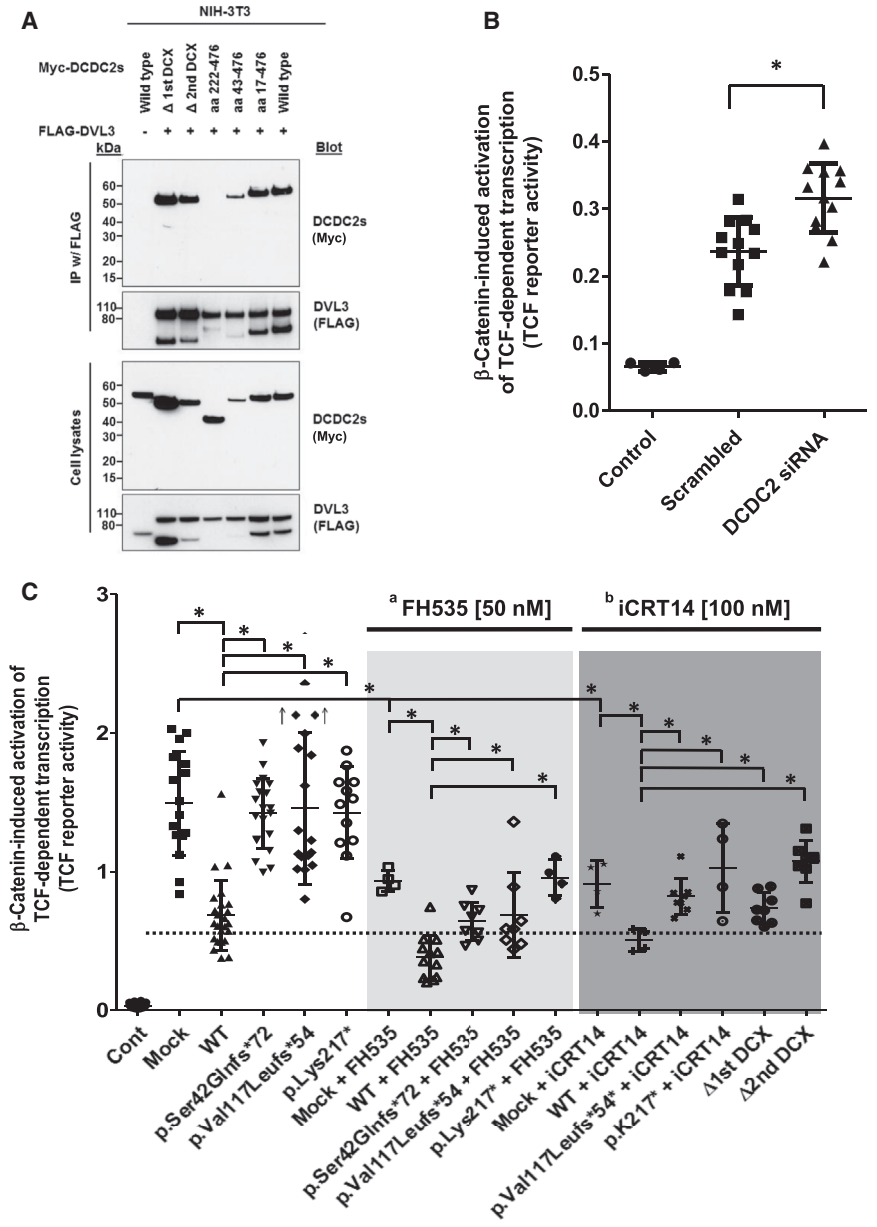

Figure 2. DCDC2 Interacts with Dishevelled and Inhibits β-Catenin-Dependent Wnt Signaling Synergistically with Wnt Inhibitors

(A) DCDC2 interacts with DVL3 when both are transiently overexpressed in NIH 3T3 cells. A construct (aa 222-476) lacking both doublecortin (DCX) domains (see Figure S2 for constructs) does not interact with DVL3, whereas the deletion of either DCX domain alone is not sufficient to abrogate the interaction.

(B) Knockdown of *DCDC2* in NIH 3T3 activates the β-catenin-dependent WNT pathway. Cells were transfected with an empty vector pcDNA3 (Control) or pcDNA3-S33Y-β-catenin together with scrambled or *DCDC2* siRNA. The ratio between the luciferase activity obtained from the cotransfected TCF-responsive reporter and the control luciferase reporter gene construct (pGL4.74[hRluc/YK]) was calculated and designated as "TCF reporter activity."

(C) Cells were transfected with an empty vector pcDNA3 (Control) or pcDNA3-S33Y-β-catenin (Mock) together with *DCDC2* constructs. Left panel: Overexpression of WT, but not mutant, *DCDC2* inhibits β-catenin-induced activation of TCF-dependent reporter gene. Light gray panel: The Wnt inhibitor FH535 suppresses TCF reporter activity. Overexpression of WT *DCDC2*, but not three mutant *DCDC2* clones, inhibits TCF reporter activity additively to the effect of FH535. Dark gray panel: Likewise, the Wnt inhibitor iCRT14 suppresses TCF reporter activity. Overexpression of WT *DCDC2*, but not mutants, inhibits TCF reporter activity additively to the effect of iCRT14. Two cDNA clones lacking the first or second DCX domain, respectively (Δ1st DCX and Δ2nd DCX), also fail to suppress TCF reporter activity. A dotted horizontal line is drawn for easier interpretation of results. ↑ indicates two outliers at 2.4 and 2.7. [a]FH535 (middle light gray panel) is known to suppress β-catenin/TCF-mediated transcription and to inhibit β-catenin and GRIP-1 recruitment to PPARγ; [b]iCRT14 (left dark gray panel) is known to modulate interaction between β-catenin and TCF and inhibit β-catenin/TCF-mediated transcription.

recapitulate the spheroid defects commonly observed after the loss of function of other NPHP proteins.[1,24]

Because loss of *Dcdc2* constitutively activates Wnt signaling (Figure 2B), we hypothesized that treating spheroids grown from renal cells depleted for *Dcdc2* with Wnt inhibitors would restore the frequency of cilia. We grew IMCD3 spheroids in the presence of either 50 nM FH535 or 100 nM iCRT14 for 72 hr and scored for cilia per nucleus in 3D structures. The cells exposed to 50 nM FH535 failed to thrive and resulted in no viable spheroids (data not shown). However, the cells treated with 100 nM iCRT14 did generate well-polarized spheroids with lumens. The Wnt inhibitor treatment noticeably rescued the effects of *Dcdc2* knockdown in the cells growing in 3D structures by restoring cilia numbers (Figures 3C and 3D). This suggests a role for Wnt signaling in the process of ciliation.

Dcdc2 Knockdown Replicates Ciliopathy Phenotypes in Zebrafish

To examine the renal cystic phenotype in an in vivo vertebrate model, we studied loss-of-function of *dcdc2b* in zebrafish using a morpholino targeted against the start codon (AUGMO) to suppress the translation of *dcdc2b* mRNA. The knockdown efficiency of the AUGMO was dose dependent, producing clear visible phenotypes in higher percentage of embryos at 200 μM. In comparison with WT control embryos, knockdown of *dcdc2b* resulted in typical ciliopathy-related defects such as ventrally curved body axis, hydrocephalus, kidney cysts, kinky tails, and

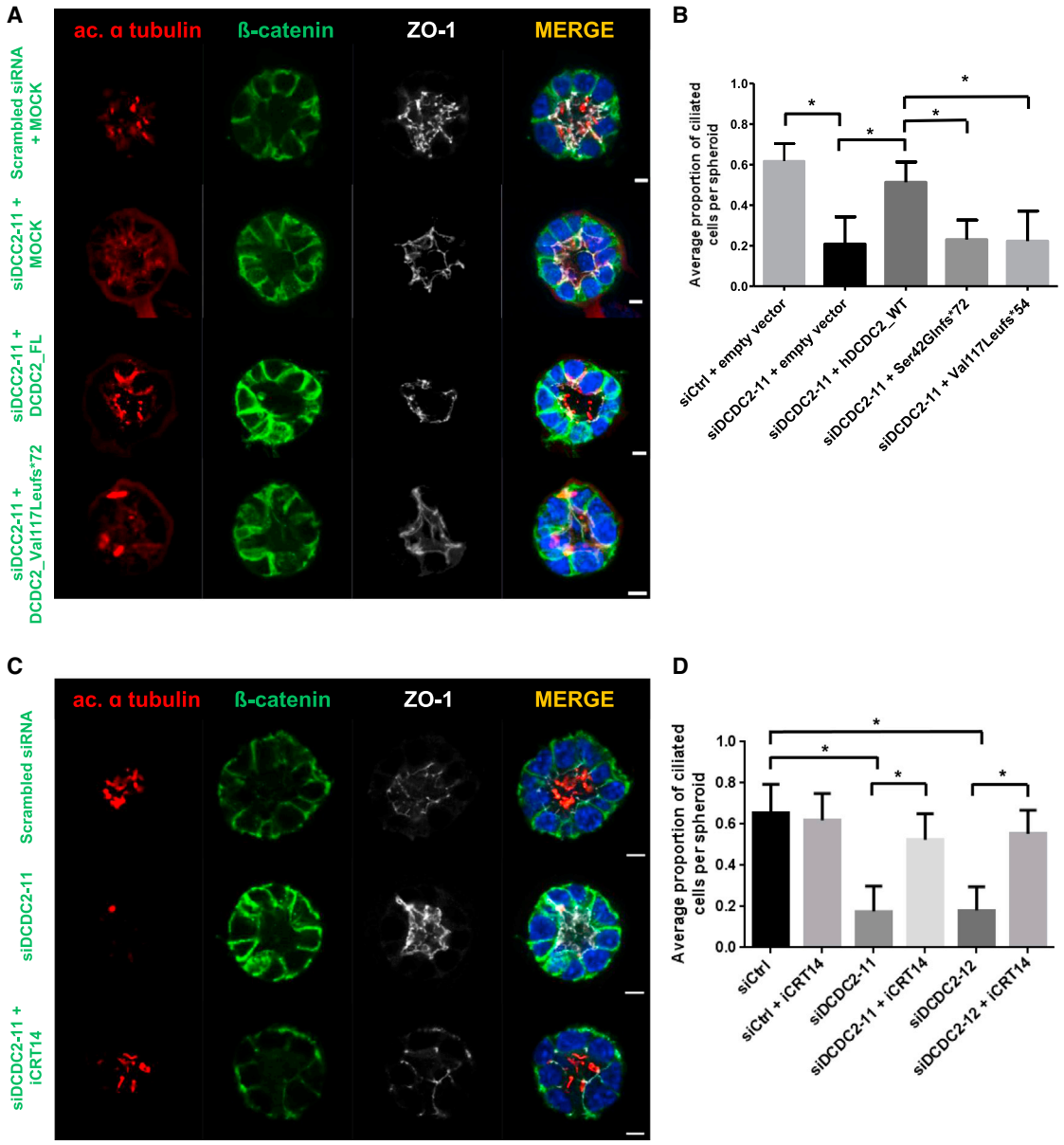

Figure 3. Lack of *Dcdc2* Is Rescued by Full-Length *DCDC2* and by Wnt Inhibition, but Not by Mutants Detected in NPHP-RC

(A) siRNA (siDcdc2-11) mediated knockdown of *Dcdc2* in IMCD3 cells grown in 3D spheroid culture causes a ciliogenesis defect that is rescued by overexpression of human WT *DCDC2*, but not by mutants found in humans with NPHP-RC. For each condition >50 spheroids were evaluated for the percentage of ciliated cells and the experiment was repeated three times independently. Note that the red structures visible in the mutant-transfected spheroid are midbodies of dividing cells, not cilia. Scale bars are 5 μm.

(B) Ratio of ciliated cells per nuclei within each spheroid upon knockdown and after attempted rescue with WT *DCDC2* and two mutants. *$p < 0.001$, as determined by ANOVA analysis. Experiments were repeated at least two times independently and the data combined. Graphs show mean value and standard error of the mean (SEM).

(C) The ciliogenesis defect was rescued by growing spheroids in medium treated with Wnt inhibitor iCRT14 (100 μM). Scale bars are 5 μm.

(D) Quantification for two siRNAs of rescue of ciliogenesis defect by iCRT14 treatment. *$p < 0.001$, as determined by ANOVA analysis. Experiments were repeated at least two times independently and the data combined. Graphs show mean value and SEM.

occasionally pericardial edema (Figure 4). At 2 days postfertilization (dpf), 81% of the morphants showed body-axis defects with kinks or waviness in the tail (Figure 4A). Hydrocephalus was observed in 58% of morphants at 2 dpf, and kidney cysts were prominantly visible in 31% of the morphants at 3.5 dpf (Figures 4A–4C). In addition, *dcdc2b* morphants also showed malformation in otolith assembly (Figure S14). Compared to control embryos that normally had two otoliths, some of the *dcdc2b* morphants had one or two fused or three otoliths (Figure S14F). These results demonstrate that *dcdc2b* in zebrafish might have a vital role in cilia formation or function.

We further observed that suppression of *dcdc2b* caused laterality defects in liver, gut, and pancreas, which was

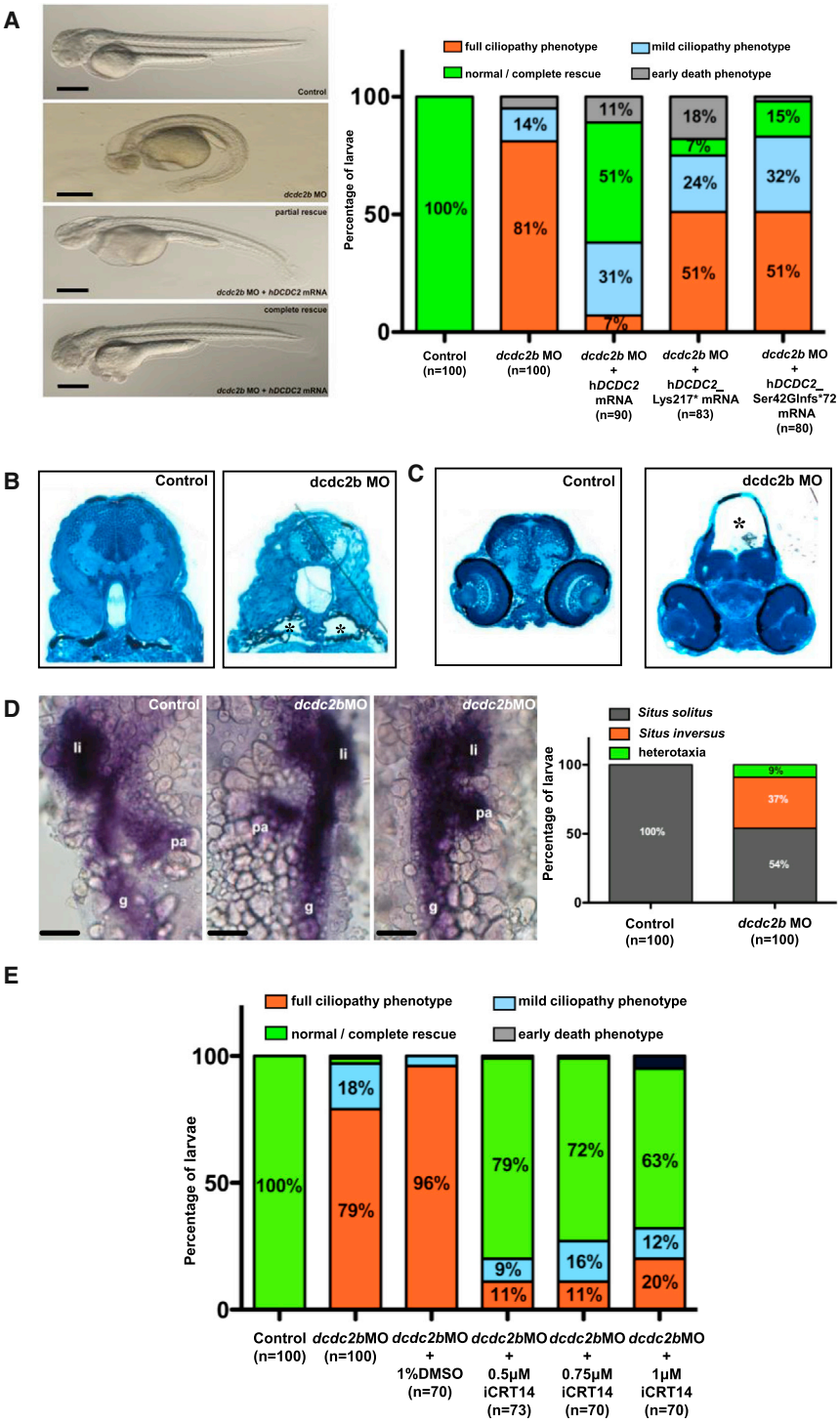

Figure 4. MO Knockdown of *dcdc2b* Replicates Ciliopathy Phenotypes in Zebrafish that Cannot Be Rescued by cDNA Clones Representing Human Ciliopathy Mutants

(A) Zebrafish embryos injected with AUGMO at one-cell stage produced defects characteristic of cilia dysfunction. Lateral view of 2-day-old control and morphant embryos. *dcdc2b* morphant developed ventrally bent body axis, hydrocephalus, tail kinks, and pericardial edema ("full ciliopathy phenotype"). Morphologically visible ciliopathy phenotypes in *dcdc2b* morphants were completely or partially rescued (lacking at least one phenotype) by coinjection of 5′capped mRNA of WT human *DCDC2*. Coinjection of AUGMO with capped mRNA of either of the two human *DCDC2* mutant clones h*DCDC2_Lys217** or h*DCDC2_Ser42Glnfs*72* mostly failed to rescue ciliary defects. Scale bar is 100 μm.

(B) Histological sections of pronephros from control and morphant embryo at 3.5 dpf. *dcdc2b* morphants clearly showed dilation of the pronephric duct (asterisks) compared to control embryos.

(C) Transverse brain sections shows hydrocephalus (asterisk) in *dcdc2b* morphants as compared to control brain sections (methylene blue and silver stain).

(D) Left-right asymmetry defects in liver, gut, and pancreas as visualized by in situ hybridization for the expression of *foxa3* with quantitation by histogram (li, liver; pa, pancreas; g, gut). Scale bar is 50 μm.

(E) Treatment with β-catenin inhibitor iCRT14 within the dose range of 0.5–1 μM rescued *dcdc2b* knockdown ciliopathy phenotypes in the morphants.

Histograms are representation of two or three independent experiments.

visualized by whole-mount in situ hybridization for the expression of *foxa3* (Figure 4D). Interestingly, immunohistochemical staining with an anti-acetylated tubulin antibody revealed that knockdown of *dcdc2b* does not alter motile cilia length in zebrafish kidney or spinal cord (Figure S14A–S14D). Electronmicrographs of the motile pronephric cilia of *dcdc2b* morphants showed no structural defects in comparison to WT pronephric cilia (Figure S14E).

To confirm the specificity of the phenotype and to determine whether the biological function of DCDC2 is evolutionarily conserved between human and zebrafish, we performed an mRNA rescue experiment by coinjecting human WT *DCDC2* mRNA along with *dcdc2b* MO into one-cell-stage embryos. Injection of WT human *DCDC2* mRNA rescued morphologically visible ciliary phenotypes in 51% of the morphants, suggesting a similar role for *dcdc2b* as for DCDC2 in cilia function (Figure 4A). We further tested the pathogenicity of the *DCDC2* mutations identified in individuals diagnosed for NPHP-RC by a similar rescue approach where *dcdc2b* MO was coinjected with capped mRNA of the human mutation representing clones hDCDC2_Lys217* or hDCDC2_Ser42Glnfs*72 into one-cell-stage embryos. Both mutations were unable to completely rescue the phenotype of *dcdc2b* morphants, confirming that these

mutations indeed affect the function of the protein (Figure 4A).

Zebrafish Ciliopathy Phenotype Is Rescued by a β-Catenin Inhibitor

Since knockdown or overexpression of *Dcdc2* in NIH 3T3 cells altered the Wnt/β-catenin pathway, we hypothesized that the ciliopathy phenotype observed in zebrafish *dcdc2b* morphants might be a result of derailed Wnt signaling pathway. To test this hypothesis, we exposed the morphants to 0.5 μM, 0.75 μM, and 1 μM of a potent β-catenin inhibitor, iCRT14 at the beginning of gastrulation. After 48 hr period of exposure, the embryos were scored for body curvature, hydrocephalus, tail kinks, and pericardial edema. Interestingly, iCRT14 was able to effectively rescue the phenotype in higher percentage of embryos at doses ranging from 0.5 to 1 μM (Figure 4E). However, concentrations higher than 1 μM were toxic to the embryos (data not shown). Our in vivo and in vitro results strongly suggest a role of Wnt signaling pathway in the pathogenesis of NPHP-RC.

Discussion

We here identified mutations of *DCDC2* as a previously unknown cause of a renal-hepatic ciliopathy in humans that is characterized by severe early-onset liver fibrosis within the first year of life. DCDC2 localized to the ciliary axoneme and to mitotic spindle fibers in a cell-cycle-dependent manner. We showed that DCDC2 interacts with DVL, and *DCDC2* overexpression inhibited β-catenin-dependent Wnt signaling in an effect additive to Wnt inhibitors. Mutations detected in human NPHP-RC lacked these effects. A Wnt inhibitor restored ciliogenesis in 3D IMCD3 cultures, emphasizing the importance of Wnt signaling for renal tubulogenesis. The fact that knockdown of DCDC2 reduces the number of cilia in cell culture, but not in dcdc2b zebrafish morphants might be explained by the biological differences between primary cilia of IMCD3 cells and multiciliated, motile cilia of zebrafish larval pronephric duct. Finally, knockdown of *dcdc2b* in zebrafish recapitulated NPHP-RC phenotypes, which were rescued by a Wnt inhibitor and by WT but not by mutant *DCDC2*. We thus demonstrate a central role of Wnt signaling in the pathogenesis of NPHP-RC, suggesting an avenue for potential treatment of NPHP-RC.

Broad pleiotropy is a common feature of NPHP-RC. In this context, the absence of renal involvement in individual A4435-21 at 9 years of age does not exclude that the affected individual might develop renal involvement later in life, because individual A3547-22 developed chronic kidney disease at 14 years of age with no signs of renal involvement earlier in life. Due to the significant overlap of the observed phenotype with other forms of NPHP-RC we introduce the term "NPHP19" for this variant of NPHP-RC.

By immunofluorescence studies, we show that DCDC2 localizes to the ciliary axoneme and to mitotic spindle fibers. This localization pattern is clearly distinct from other NPHP-RC proteins, such as CEP164 and SDCCAG8 (Figures S6 and S7), which preferentially stain the basal body and the mitotic spindle poles. Interestingly, the interaction partners of DCDC2, DVL3 and JIP1,[34] and KIF3a[31] show a localization pattern that resembles CEP164 and SDCCAG8. The finding that there was no tight subcellular colocalization for these proteins could be due to the fact that the proteins bind to tubulin as suggested by Figure S8. The specific subcellular compartments to which NPHP-RC proteins localize are very small and often extremely dynamic during different phases of cell cycle, making colocalization experiments difficult to interpret. This holds true for many of the >90 NPHP-RC that are known so far.

Our in vitro studies in cell lines, spheroids, and our in vivo studies in zebrafish clearly demonstrate a role of increased canonical Wnt signaling in the pathogenesis of NPHP-RC. Loss-of-function mutations observed in individuals with NPHP-RC fail to reduce canonical Wnt signaling in vitro. The zebrafish phenotype observed upon knockdown of *dcdc2b* is reminiscent of the one seen in the zebrafish $apc^{-/-}$ mutant, a model of constitutively activated Wnt.[39] The fact that the phenotype of *dcdc2b* zebrafish morphants could be mitigated by treatment with Wnt inhibitors further supports the significance of dysregulated canonical Wnt signaling in this model.

Consistent with the observed human phenotype, our histological studies of $Dcdc2^{-/-}$ mice reveal periportal liver fibrosis and demonstrate biliary duct proliferation and extensive collagen deposition surrounding the portal tracts compared to WT control (Figure S3). It has been frequently reported that Wnt signaling regulates tubule formation (reviewed in [40]). Interestingly, the role of Wnt/β-catenin signaling during the development of liver fibrosis was recently analyzed.[41] It was shown that abnormal activation of Wnt/β-catenin signaling promotes tissue fibrogenesis while downregulation of Wnt signaling suppresses the activity of hepatic stellate cells and the collagen synthesis. Our data suggest that loss of DCDC2 function does not profoundly affect renal tubulogenesis but renders the tubules more responsive to Wnt modulation in the 3D polarized tubule state. Activated Wnt signaling has so far been implicated in human NPHP-RC in the presence of *INVS* mutations.[4] Our demonstration that Wnt inhibitors reverse the failure of *DCDC2* mutants to reduce canonical Wnt signaling opens a potential route toward treatment for certain forms of NPHP-RC.

Supplemental Data

Supplemental Data include fourteen figures and three tables and can be found with this article online at http://www.cell.com/ajhg.

Acknowledgments

We are grateful to families and study individuals for their contribution. We would like to thank Milan Elleder and Helena Hůlkova (Institute for Inherited Metabolic Disorders) for histological preparation of liver biopsy specimen. We thank the zebrafish core facility, Karolinska Institutet for providing zebrafish embryos. We thank Kjell Hultenby, Eva Blomen, and Sally Cheung for technical support. We thank the Live Cell Imaging unit/Nikon Center of Excellence, Department of Biosciences and Nutrition, Karolinska Institutet for their support. This research was supported by grants from the National Institutes of Health to F.H. (DK1069274, DK1068306, DK064614), to P.C.H. (DK090728, DK059597), to R.A. (DK099434), and by the CIHR to L.P. (MOP130507). H.Y.G. is supported by the NephCure Foundation and by the ASN Foundation for Kidney Research. T.H. was supported by General University Hospital program RVO-VFN 64165/2012. This work was in part supported by grants to J.K. from Knut and Alice Wallenberg Foundation, the Swedish Research Council, the Centre for Biosciences, the Centre for Innovative Medicine, and Jonasson donation to the School of Technology and Health, Kungliga Tekniska Högskolan, Swedish Brain Foundation (Hjärnfonden) and Swedish Brain Foundations postdoc fellowship award to G.C., from the European Union Framework Programmes 241955 "SYSCILIA" and 305608 "EURenOmics" as well as the Dutch Kidney Foundation grants CP11.18 "KOUNCIL"/13A3D103 to R.H.G., and from the Deutsche Forschungs–gemeinschaft to K.Z. (ZE 205/14-1). F.H. is an Investigator of the Howard Hughes Medical Institute, a Doris Duke Distinguished Clinical Scientist, and the Warren E. Grupe Professor.

Received: September 30, 2014
Accepted: December 3, 2014
Published: December 31, 2014

Web Resources

ExAC Browser Beta, http://exac.broadinstitute.org
Online Mendelian Inheritance in Man (OMIM), http://www.omim.org/
UCSC Genome Bioinformatics, http://genome.ucsc.edu/

References

1. Sang, L., Miller, J.J., Corbit, K.C., Giles, R.H., Brauer, M.J., Otto, E.A., Baye, L.M., Wen, X., Scales, S.J., Kwong, M., et al. (2011). Mapping the NPHP-JBTS-MKS protein network reveals ciliopathy disease genes and pathways. Cell *145*, 513–528.
2. Hildebrandt, F., Benzing, T., and Katsanis, N. (2011). Ciliopathies. N. Engl. J. Med. *364*, 1533–1543.
3. Hildebrandt, F., Otto, E., Rensing, C., Nothwang, H.G., Vollmer, M., Adolphs, J., Hanusch, H., and Brandis, M. (1997). A novel gene encoding an SH3 domain protein is mutated in nephronophthisis type 1. Nat. Genet. *17*, 149–153.
4. Otto, E.A., Schermer, B., Obara, T., O'Toole, J.F., Hiller, K.S., Mueller, A.M., Ruf, R.G., Hoefele, J., Beekmann, F., Landau, D., et al. (2003). Mutations in INVS encoding inversin cause nephronophthisis type 2, linking renal cystic disease to the function of primary cilia and left-right axis determination. Nat. Genet. *34*, 413–420.
5. Attanasio, M., Uhlenhaut, N.H., Sousa, V.H., O'Toole, J.F., Otto, E., Anlag, K., Klugmann, C., Treier, A.C., Helou, J., Sayer, J.A., et al. (2007). Loss of GLIS2 causes nephronophthisis in humans and mice by increased apoptosis and fibrosis. Nat. Genet. *39*, 1018–1024.
6. Chaki, M., Airik, R., Ghosh, A.K., Giles, R.H., Chen, R., Slaats, G.G., Wang, H., Hurd, T.W., Zhou, W., Cluckey, A., et al. (2012). Exome capture reveals ZNF423 and CEP164 mutations, linking renal ciliopathies to DNA damage response signaling. Cell *150*, 533–548.
7. Zhou, W., Otto, E.A., Cluckey, A., Airik, R., Hurd, T.W., Chaki, M., Diaz, K., Lach, F.P., Bennett, G.R., Gee, H.Y., et al. (2012). FAN1 mutations cause karyomegalic interstitial nephritis, linking chronic kidney failure to defective DNA damage repair. Nat. Genet. *44*, 910–915.
8. Olbrich, H., Fliegauf, M., Hoefele, J., Kispert, A., Otto, E., Volz, A., Wolf, M.T., Sasmaz, G., Trauer, U., Reinhardt, R., et al. (2003). Mutations in a novel gene, *NPHP3*, cause adolescent nephronophthisis, tapeto-retinal degeneration and hepatic fibrosis. Nat. Genet. *34*, 455–459.
9. Otto, E., Hoefele, J., Ruf, R., Mueller, A.M., Hiller, K.S., Wolf, M.T., Schuermann, M.J., Becker, A., Birkenhäger, R., Sudbrak, R., et al. (2002). A gene mutated in nephronophthisis and retinitis pigmentosa encodes a novel protein, nephroretinin, conserved in evolution. Am. J. Hum. Genet. *71*, 1161–1167.
10. Mollet, G., Salomon, R., Gribouval, O., Silbermann, F., Bacq, D., Landthaler, G., Milford, D., Nayir, A., Rizzoni, G., Antignac, C., and Saunier, S. (2002). The gene mutated in juvenile nephronophthisis type 4 encodes a novel protein that interacts with nephrocystin. Nat. Genet. *32*, 300–305.
11. Otto, E., Loeys, B., Khanna, H., Hellemans, J., Sudbrak, R., Fan, S., Muerb, U., O'Toole, J.F., Helou, J., Attanasio, M., et al. (2005). A novel ciliary IQ domain protein, NPHP5, is mutated in Senior-Loken syndrome (nephronophthisis with retinitis pigmentosa), and interacts with RPGR and calmodulin. Nat. Genet. *37*, 282–288.
12. Sayer, J.A., Otto, E.A., O'Toole, J.F., Nurnberg, G., Kennedy, M.A., Becker, C., Hennies, H.C., Helou, J., Attanasio, M., Fausett, B.V., et al. (2006). The centrosomal protein nephrocystin-6 is mutated in Joubert syndrome and activates transcription factor ATF4. Nat. Genet. *38*, 674–681.
13. Valente, E.M., Silhavy, J.L., Brancati, F., Barrano, G., Krishnaswami, S.R., Castori, M., Lancaster, M.A., Boltshauser, E., Boccone, L., Al-Gazali, L., et al.; International Joubert Syndrome Related Disorders Study Group (2006). Mutations in CEP290, which encodes a centrosomal protein, cause pleiotropic forms of Joubert syndrome. Nat. Genet. *38*, 623–625.
14. Delous, M., Baala, L., Salomon, R., Laclef, C., Vierkotten, J., Tory, K., Golzio, C., Lacoste, T., Besse, L., Ozilou, C., et al. (2007). The ciliary gene RPGRIP1L is mutated in cerebello-oculo-renal syndrome (Joubert syndrome type B) and Meckel syndrome. Nat. Genet. *39*, 875–881.
15. Otto, E.A., Trapp, M.L., Schultheiss, U.T., Helou, J., Quarmby, L.M., and Hildebrandt, F. (2008). NEK8 mutations affect ciliary and centrosomal localization and may cause nephronophthisis. J. Am. Soc. Nephrol. *19*, 587–592.
16. Halbritter, J., Diaz, K., Chaki, M., Porath, J.D., Tarrier, B., Fu, C., Innis, J.L., Allen, S.J., Lyons, R.H., Stefanidis, C.J., et al. (2012). High-throughput mutation analysis in patients with a nephronophthisis-associated ciliopathy applying multiplexed barcoded array-based PCR amplification and next-generation sequencing. J. Med. Genet. *49*, 756–767.
17. Halbritter, J., Porath, J.D., Diaz, K.A., Braun, D.A., Kohl, S., Chaki, M., Allen, S.J., Soliman, N.A., Hildebrandt, F., and

Otto, E.A.; GPN Study Group (2013). Identification of 99 novel mutations in a worldwide cohort of 1,056 patients with a nephronophthisis-related ciliopathy. Hum. Genet. *132*, 865–884.
18. Kruglyak, L., Daly, M.J., Reeve-Daly, M.P., and Lander, E.S. (1996). Parametric and nonparametric linkage analysis: a unified multipoint approach. Am. J. Hum. Genet. *58*, 1347–1363.
19. Strauch, K., Fimmers, R., Kurz, T., Deichmann, K.A., Wienker, T.F., and Baur, M.P. (2000). Parametric and nonparametric multipoint linkage analysis with imprinting and two-locus-trait models: application to mite sensitization. Am. J. Hum. Genet. *66*, 1945–1957.
20. Gudbjartsson, D.F., Jonasson, K., Frigge, M.L., and Kong, A. (2000). Allegro, a new computer program for multipoint linkage analysis. Nat. Genet. *25*, 12–13.
21. Hildebrandt, F., Heeringa, S.F., Rüschendorf, F., Attanasio, M., Nürnberg, G., Becker, C., Seelow, D., Huebner, N., Chernin, G., Vlangos, C.N., et al. (2009). A systematic approach to mapping recessive disease genes in individuals from outbred populations. PLoS Genet. *5*, e1000353.
22. Boyden, L.M., Choi, M., Choate, K.A., Nelson-Williams, C.J., Farhi, A., Toka, H.R., Tikhonova, I.R., Bjornson, R., Mane, S.M., Colussi, G., et al. (2012). Mutations in kelch-like 3 and cullin 3 cause hypertension and electrolyte abnormalities. Nature *482*, 98–102.
23. Zariwala, M.A., Gee, H.Y., Kurkowiak, M., Al-Mutairi, D.A., Leigh, M.W., Hurd, T.W., Hjeij, R., Dell, S.D., Chaki, M., Dougherty, G.W., et al. (2013). ZMYND10 is mutated in primary ciliary dyskinesia and interacts with LRRC6. Am. J. Hum. Genet. *93*, 336–345.
24. Otto, E.A., Hurd, T.W., Airik, R., Chaki, M., Zhou, W., Stoetzel, C., Patil, S.B., Levy, S., Ghosh, A.K., Murga-Zamalloa, C.A., et al. (2010). Candidate exome capture identifies mutation of SDCCAG8 as the cause of a retinal-renal ciliopathy. Nat. Genet. *42*, 840–850.
25. Odenthal, J., and Nüsslein-Volhard, C. (1998). fork head domain genes in zebrafish. Dev. Genes Evol. *208*, 245–258.
26. Thisse, B., Heyer, V., Lux, A., Alunni, V., Degrave, A., Seiliez, I., Kirchner, J., Parkhill, J.P., and Thisse, C. (2004). Spatial and temporal expression of the zebrafish genome by large-scale in situ hybridization screening. Methods Cell Biol. *77*, 505–519.
27. Chandrasekar, G., Vesterlund, L., Hultenby, K., Tapia-Páez, I., and Kere, J. (2013). The zebrafish orthologue of the dyslexia candidate gene DYX1C1 is essential for cilia growth and function. PLoS ONE *8*, e63123.
28. Zhou, W., and Hildebrandt, F. (2009). Molecular cloning and expression of phospholipase C epsilon 1 in zebrafish. Gene Expr. Patterns *9*, 282–288.
29. Truong, D.T., Che, A., Rendall, A.R., Szalkowski, C.E., LoTurco, J.J., Galaburda, A.M., and Holly Fitch, R. (2014). Mutation of Dcdc2 in mice leads to impairments in auditory processing and memory ability. Genes Brain Behav. *13*, 802–811.
30. Shmueli, A., Gdalyahu, A., Sapoznik, S., Sapir, T., Tsukada, M., and Reiner, O. (2006). Site-specific dephosphorylation of doublecortin (DCX) by protein phosphatase 1 (PP1). Mol. Cell. Neurosci. *32*, 15–26.
31. Massinen, S., Hokkanen, M.E., Matsson, H., Tammimies, K., Tapia-Páez, I., Dahlström-Heuser, V., Kuja-Panula, J., Burghoorn, J., Jeppsson, K.E., Swoboda, P., et al. (2011). Increased expression of the dyslexia candidate gene DCDC2 affects length and signaling of primary cilia in neurons. PLoS ONE *6*, e20580.
32. Watnick, T., and Germino, G. (2003). From cilia to cyst. Nat. Genet. *34*, 355–356.
33. Giles, R.H., van Es, J.H., and Clevers, H. (2003). Caught up in a Wnt storm: Wnt signaling in cancer. Biochim. Biophys. Acta *1653*, 1–24.
34. Coquelle, F.M., Levy, T., Bergmann, S., Wolf, S.G., Bar-El, D., Sapir, T., Brody, Y., Orr, I., Barkai, N., Eichele, G., and Reiner, O. (2006). Common and divergent roles for members of the mouse DCX superfamily. Cell Cycle *5*, 976–983.
35. Yasuda, J., Whitmarsh, A.J., Cavanagh, J., Sharma, M., and Davis, R.J. (1999). The JIP group of mitogen-activated protein kinase scaffold proteins. Mol. Cell. Biol. *19*, 7245–7254.
36. Jaeschke, A., Czech, M.P., and Davis, R.J. (2004). An essential role of the JIP1 scaffold protein for JNK activation in adipose tissue. Genes Dev. *18*, 1976–1980.
37. Caspi, M., Atlas, R., Kantor, A., Sapir, T., and Reiner, O. (2000). Interaction between LIS1 and doublecortin, two lissencephaly gene products. Hum. Mol. Genet. *9*, 2205–2213.
38. Renkema, K.Y., Stokman, M.F., Giles, R.H., and Knoers, N.V. (2014). Next-generation sequencing for research and diagnostics in kidney disease. Nat. Rev. Nephrol. *10*, 433–444.
39. Hurlstone, A.F., Haramis, A.P., Wienholds, E., Begthel, H., Korving, J., Van Eeden, F., Cuppen, E., Zivkovic, D., Plasterk, R.H., and Clevers, H. (2003). The Wnt/beta-catenin pathway regulates cardiac valve formation. Nature *425*, 633–637.
40. Miller, R.K., and McCrea, P.D. (2010). Wnt to build a tube: contributions of Wnt signaling to epithelial tubulogenesis. Developmental dynamics: an official publication of the American Association of Anatomists *239*, 77–93.
41. Ge, W.S., Wang, Y.J., Wu, J.X., Fan, J.G., Chen, Y.W., and Zhu, L. (2014). Beta-catenin is overexpressed in hepatic fibrosis and blockage of Wnt/beta-catenin signaling inhibits hepatic stellate cell activation. Molecular medicine reports *9*, 2145–2151.

The American Journal of Human Genetics

Supplemental Data

DCDC2 Mutations Cause a Renal-Hepatic Ciliopathy by Disrupting Wnt Signaling

Markus Schueler, Daniela A. Braun, Gayathri Chandrasekar, Heon Yung Gee, Timothy D. Klasson, Jan Halbritter, Andrea Bieder, Jonathan D. Porath, Rannar Airik, Weibin Zhou, Joseph J. LoTurco, Alicia Che, Edgar A. Otto, Detlef Böckenhauer, Neil J. Sebire, Tomas Honzik, Peter C. Harris, Sarah J. Koon, Meral Gunay-Aygun, Sophie Saunier, Klaus Zerres, Nadina Ortiz Bruechle, Joost P.H. Drenth, Laurence Pelletier, Isabel Tapia Pắez, Richard P. Lifton, Rachel H. Giles, Juha Kere, and Friedhelm Hildebrandt

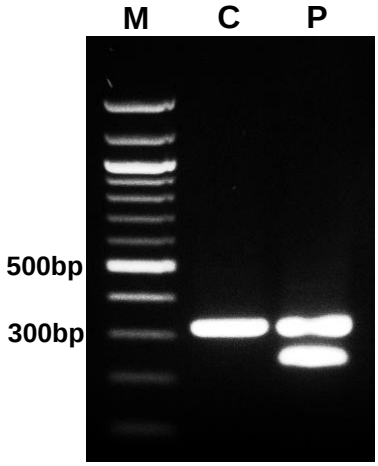

Figure S1. RT-PCR in individual A4435-21 with the c.349-2A>G mutation results in skipping of exon 4.

RT-PCR was performed on cDNA from white blood cells of A4435-21 (P) and healthy control (C) using primers 2F and 5R (see **Fig. 1C**) flanking exon 4. For healthy control a PCR product with the expected size of 323 bp was observed. In contrast, the RT-PCR of the affected individual yielded an additional PCR product of 246 bp, confirming that the detected heterozygous obligatory splice mutation c.349-2A>G results in skipping of exon 4 of *DCDC2*. Both PCR products were Sanger sequenced confirming missplicing of the *DCDC2* transcript (**Fig. 1F**). M, Marker 100 bp ladder.

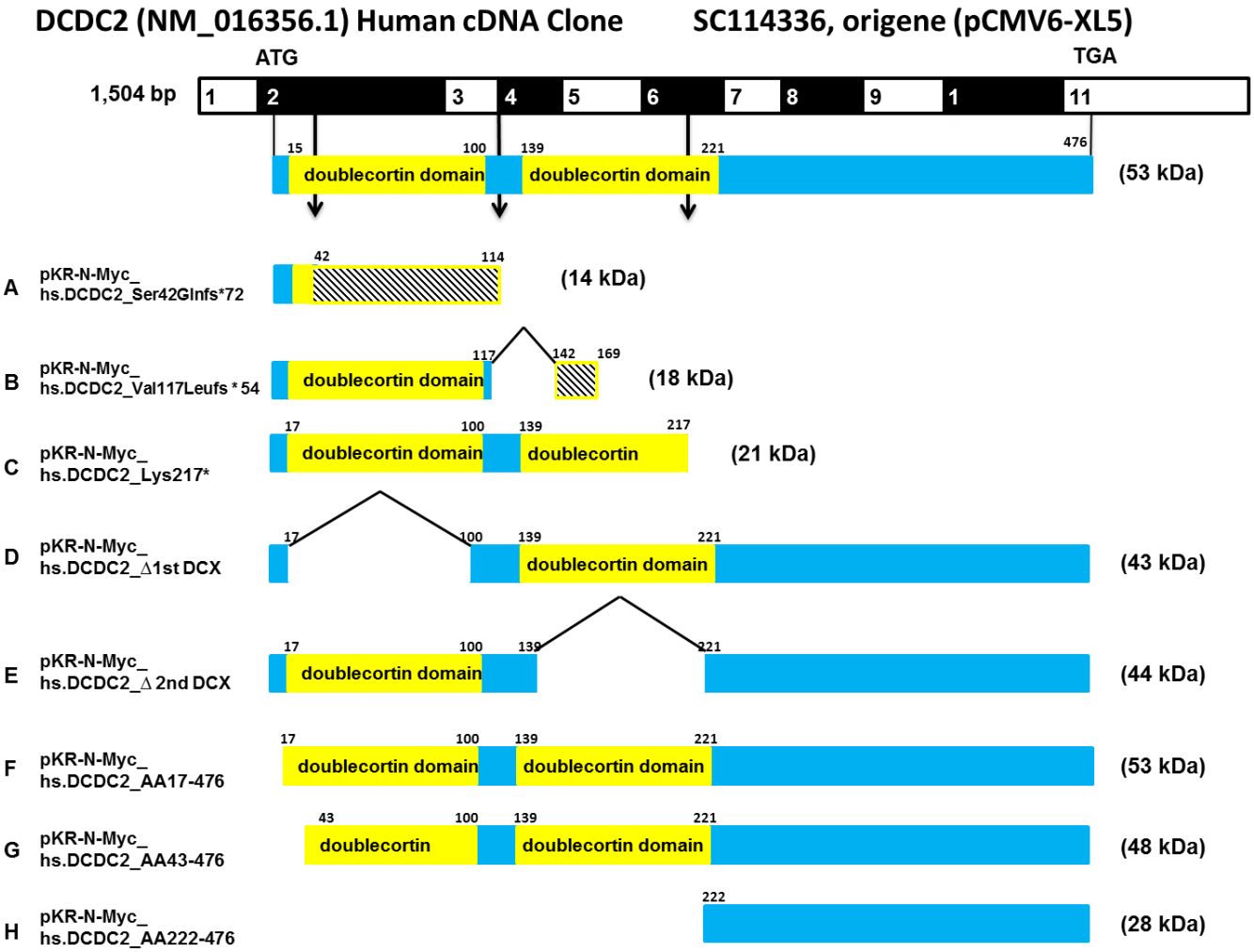

Figure S2. Domain structure of human mutations and artificial constructs in *DCDC2* .

(A) The most 5' terminal mutation causes a frameshift after 42 amino acids abrogating both doublecortin (DCX) domains.

(B) The splice site mutation causes skipping of exon 4 and a frameshift at amino acid 117 resulting in a protein truncation.

(C) The most 3' terminal mutation causes a protein truncation after 217 amino acids, resulting in a protein product that contains one complete and one partial DCX domain.

(D) An artificial construct lacking the 1st DCX domain.

(E) An artificial construct lacking the 2nd DCX domain.

(F) An artificial construct that lacks the region N terminal of the first DCX domain (first 17 amino acids).

(G) An artificial construct that lacks the first 42 amino acids that are preserved in the shortest human mutation.

(H) An artificial construct that lacks both DCX domains and contains amino acid 222 - 476 only.

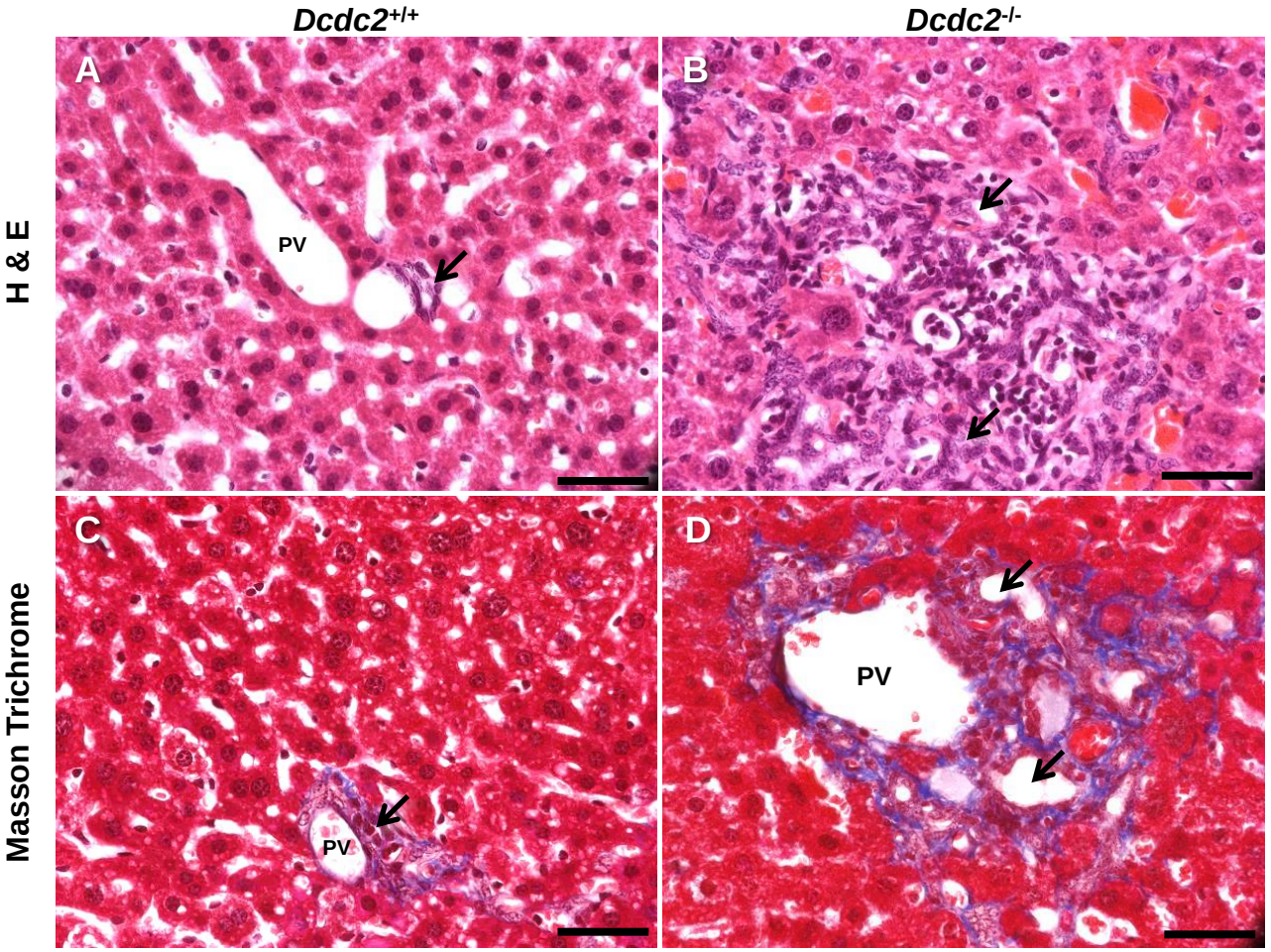

E

	Number of periportal fields with collagen deposition upon Masson Trichrome staining[1]		
Grade	**0, I**	**II, III**	**n periportal fields/animal**
***Dcdc2*$^{+/+}$ 11 months**	**7 (77.7%)**	**2 (22.2%)**	**9**
***Dcdc2*$^{-/-}$ 11 months**	**3 (27.2%)**	**8 (72.7%)**	**11**
n periportal fields	**10**	**10**	**20**

X^2=5.051 (p<0.05, 1 tailed)

[1] All periportal fields of 3 different sections from 3 different lobes per animal were evaluated.

Figure S3. Liver histology reveals periportal liver fibrosis in *Dcdc2*$^{-/-}$ mice.
Hematoxylin and eosin staining (H & E) of 11 months old *Dcdc2*$^{+/+}$ (**A**), and 11 months old *Dcdc2*$^{-/-}$ mice demonstrate biliary duct proliferation in *Dcdc2*$^{-/-}$ animals (**B**)
(**C**, **D**) Masson Trichrome staining (MTS) shows when compared to wild type control (**C**) extensive collagen deposition around the portal tracts in *Dcdc2*$^{-/-}$ animals (**D**).
(**E**) Table quantitates degree of collagen deposition within periportal fields of three different liver lobes per animal from blinded evaluation of MTS. Grades 0/I indicate presence of few collagen fibers surrounding the vessel walls and within the extracellular matrix (**C**). Grades II/III represent periportal fields with an increased deposition of collagen fibers along the circumferences of the bile ducts spreading into the liver parenchyma (**D**). Similar data were obtained from another *Dcdc2*$^{-/-}$ animal (data not shown).
Note the increased number of periportal fields ranked II or III grade in the *Dcdc2*$^{-/-}$ mice.
PV: branch of portal vein; arrow: bile duct; Scale bar: 500 µm.

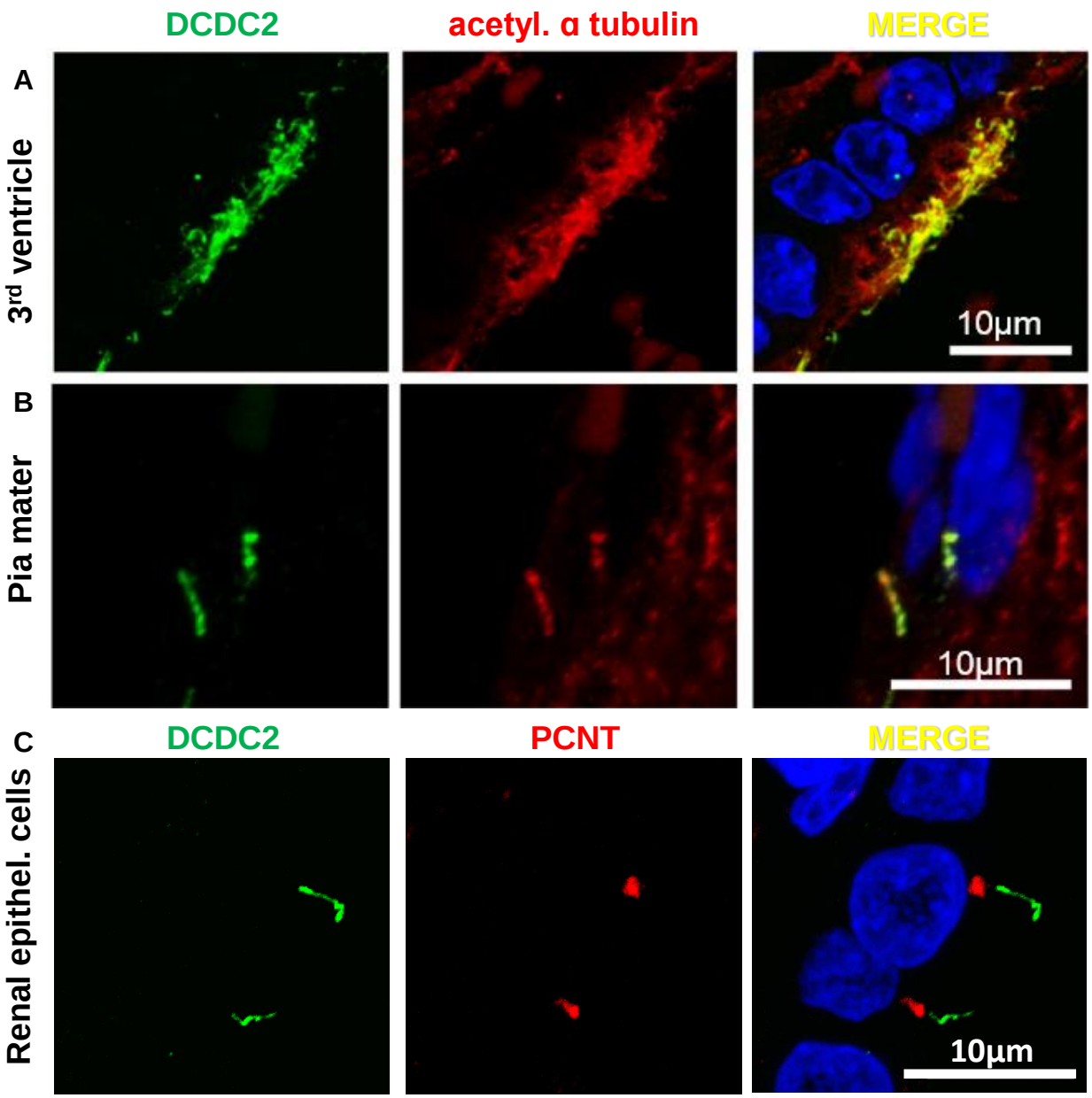

Figure S4. DCDC2 decorates the axoneme of primary cilia in ependymal cells of the third brain ventricle, and of the cranial pia mater in mice as well as of human renal epithelial cells, but does not localize to the basal body.

(**A**) DCDC2 co-localizes with acetylated-α-tubulin at the ciliary axoneme of ependymal cells in the third ventricle of the brain, (**B**) of cells in the cranial pia mater. (**C**) Axonemal localization excludes the basal body (marker PCNT) as shown in human renal epithelial cells. Coronal brain of FVB/N mice (male, 3 mo old) were fixed with 4% PFA/PBS by immersion, paraffin-embedded and sectioned. Tissue sections were blocked with 5% horse serum/0.05% PBS-Triton X-100 and immuno-stained with anti-DCDC2 antibody (green, Santa Cruz), anti-acetylated-α-tubulin antibody (red, Sigma) or anti-PCNT antibody (red, Atlas antibodies) and DRAQ5 to label DNA (blue).

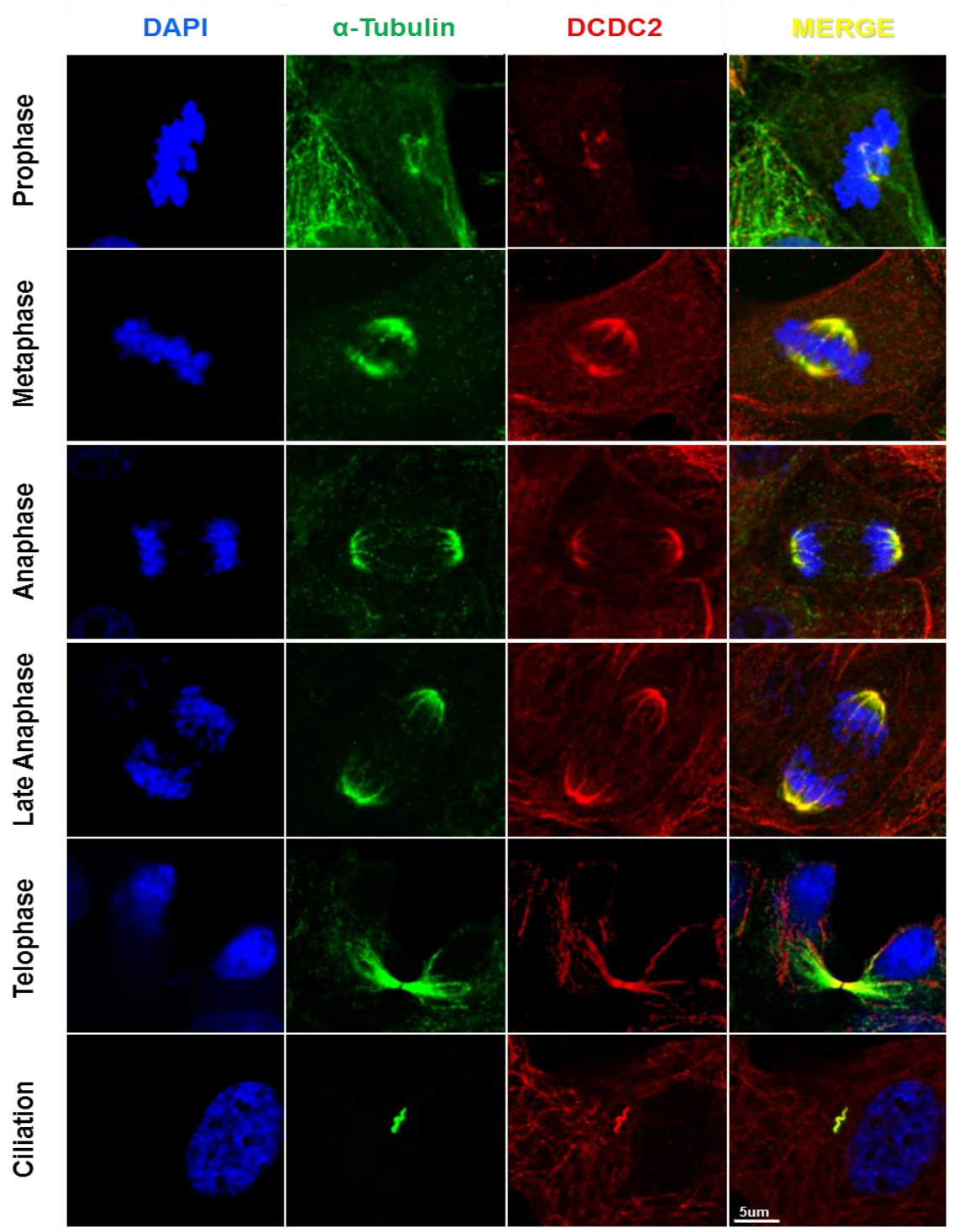

Figure S5. DCDC2 colocalizes with acetylated α-tubulin to mitotic spindle fibers and the ciliary axoneme.

DCDC2 localizes to the mitotic spindle throughout the phases of mitosis, sparing the spindle poles and the interpolar spindle fibers in metaphase. Upon serum starvation DCDC2 decorates the ciliary axoneme. In telophase it labels the abscission structure.

Cells were seeded at low density onto coverslips. For cell cycle images MDCK-II cells were grown to ~80% confluency. For ciliation images hTERT-RPE were serum starved for 48 hrs. Cells were fixed (4% PFA), permeabilized (0.1% SDS) and immuno stained with mouse anti-acetylated-α-tubulin antibody (green, abcam), rabbit anti-DCDC2 antibody (red, abcam), DAPI to label DNA (blue).

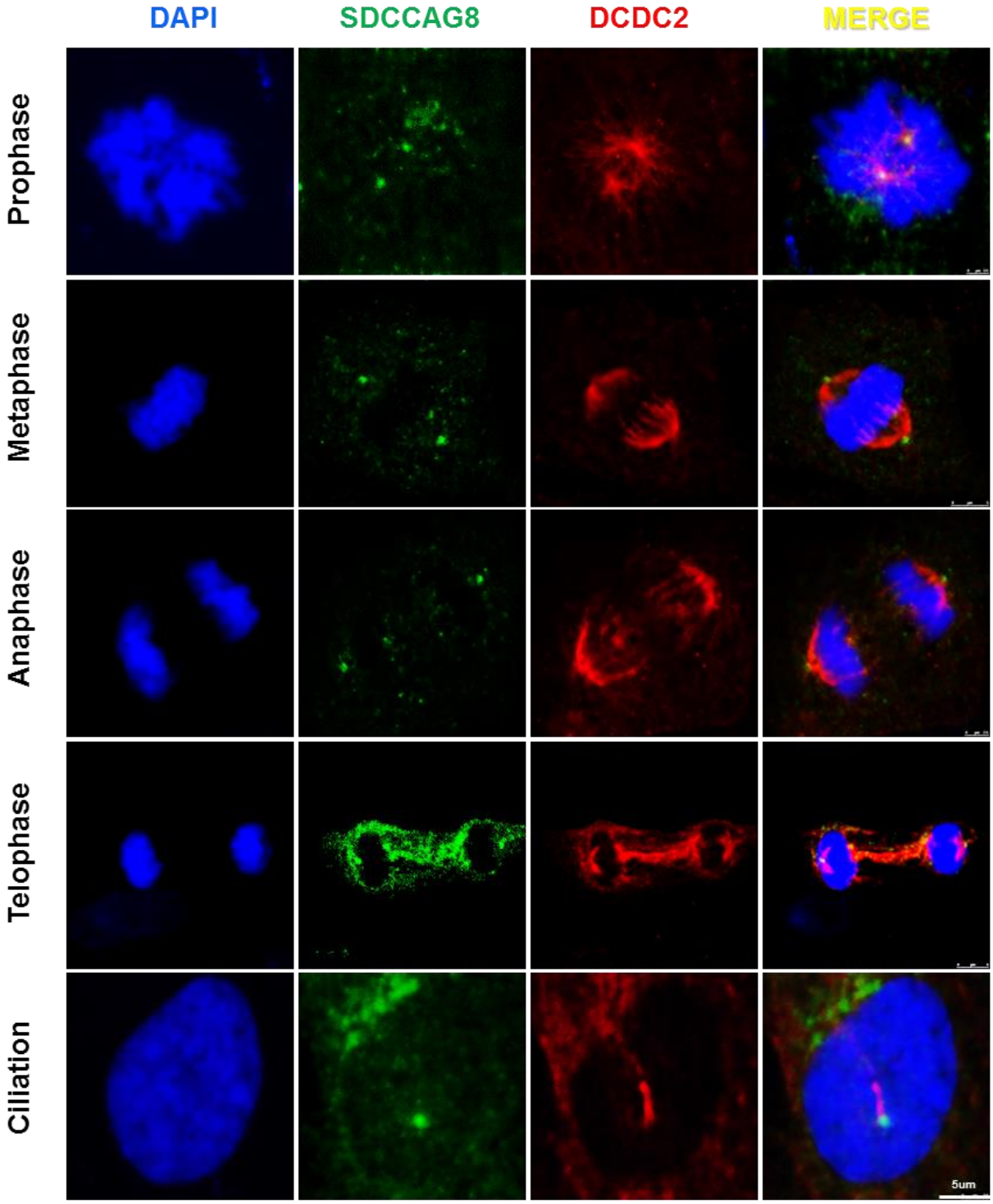

Figure S6. In contrast to the established ciliopathy protein SDCCAG8, which stains spindle poles and basal bodies, DCDC2 stains spindle microtubules and the ciliary axoneme.

hTERT-RPE1 were seeded onto coverslips, grown to confluency and serum-starved for 36 hrs. Cells were fixed (4% PFA), permeabilized (0.1% SDS), and immuno-stained with anti-SDCCAG8 (green). Costaining was performed using an anti-DCDC2 antibody (red, abcam) and DAPI to label DNA (blue).

Note that DCDC2 stains spindle fibers (metaphase and anaphase) and the entire axoneme of primary cilia ('ciliation'), but does not colocalize with the centrosomal ciliopathy protein SDCCAG8 to spindle poles or basal bodies.

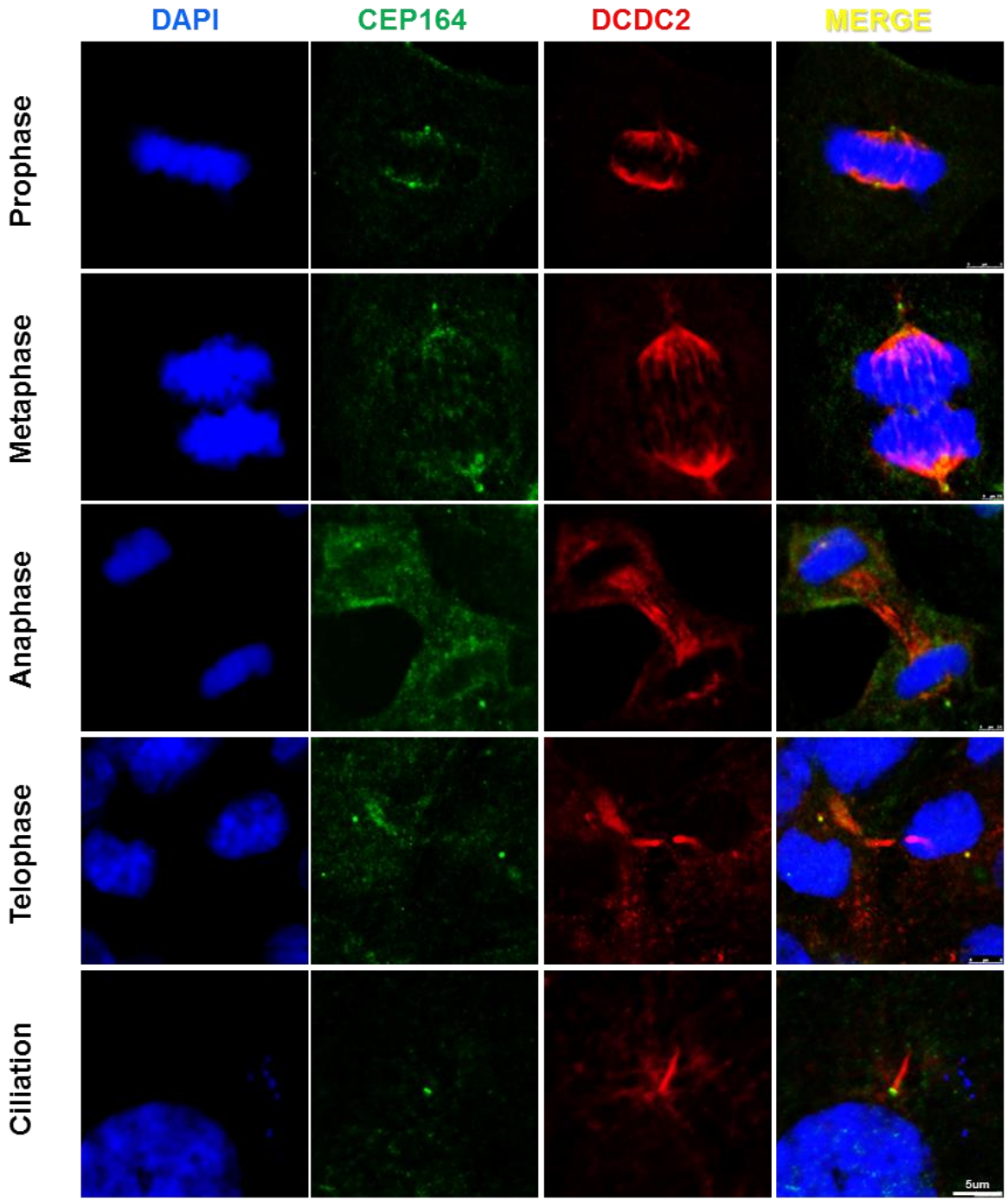

Figure S7. In contrast to the established ciliopathy protein CEP164, which stains spindle poles and basal bodies, DCDC2 stains spindle microtubules and the ciliary axoneme.

hTERT-RPE1 were treated as described before (**Suppl. Fig. 6**) and immuno-stained with anti-CEP164 antibody (green). Costaining was performed using an anti-DCDC2 antibody (red, abcam) and DAPI to label DNA (blue).

Note that DCDC2 stains spindle fibers (metaphase and anaphase) and the entire axoneme of primary cilia, but does not colocalize with the centrosomal ciliopathy protein CEP164 to spindle poles or basal bodies.

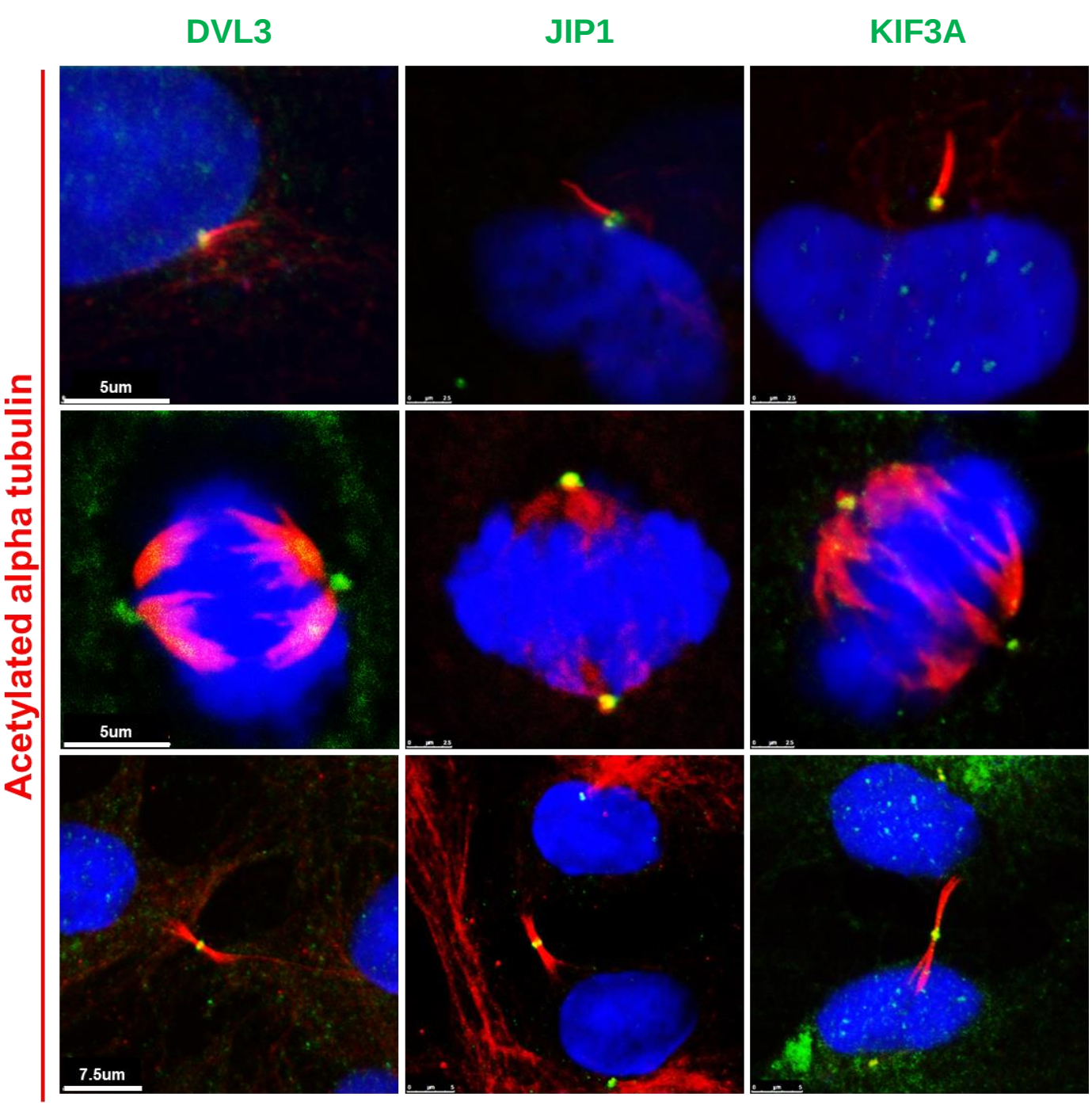

Figure S8. Interaction partners of DCDC2 show a similar localization pattern throughout cell cycle.

The localization pattern of the interacting proteins DVL3, JIP1, and KIF3A was analyzed in comparison to acetylated alpha tubulin in ciliated cells, in metaphase and cytokinesis. All three proteins colocalize to the basal body, the mitotic spindle poles and the midbody.

hTERT-RPE1 cells were seeded on coverglasses, grown to confluency and serum starved for 48 hrs to induce ciliation. Fixation and permeabilization was done using aceton, DAPI was used to stain nuclei.

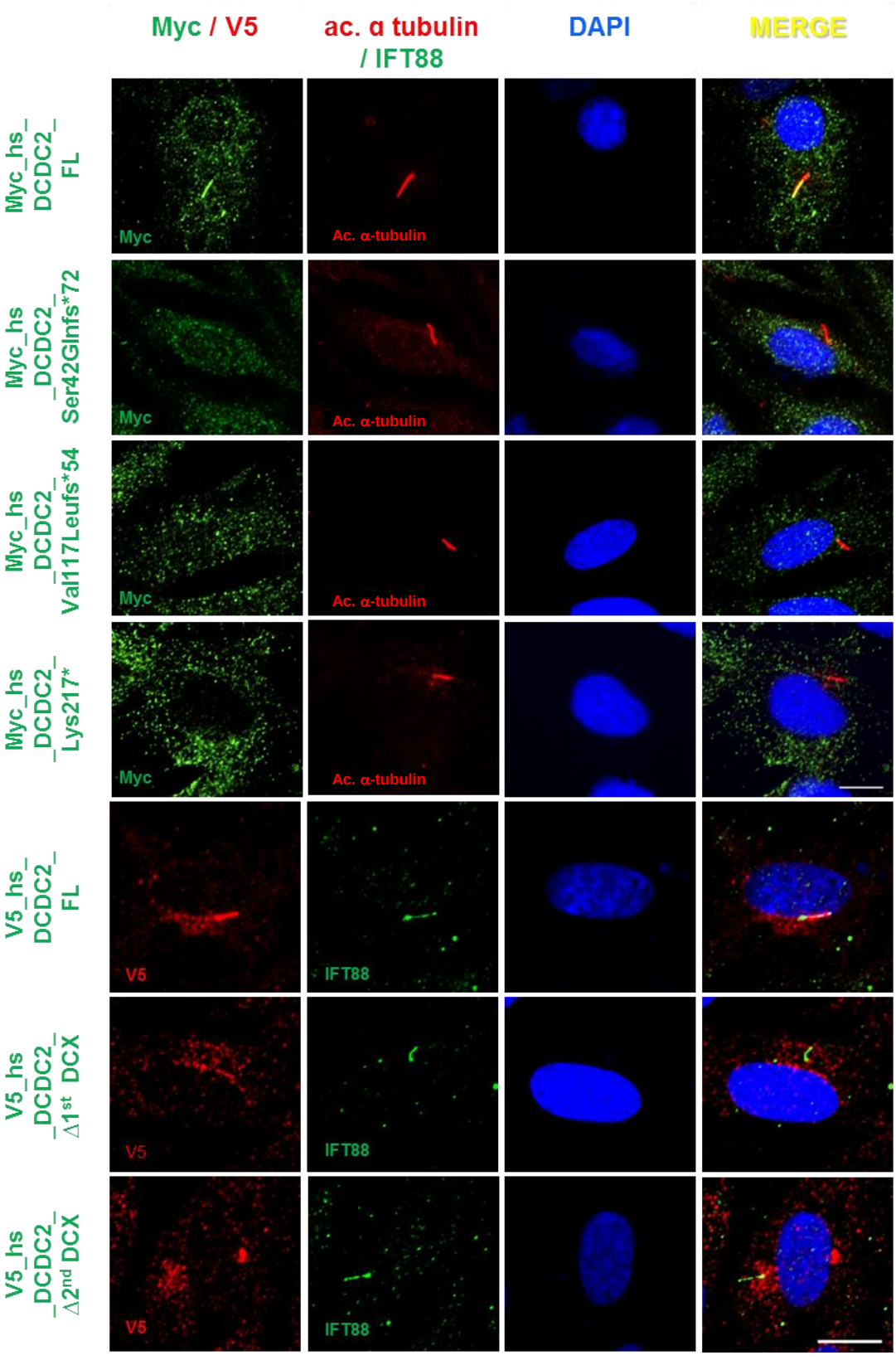

Figure S9. Wildtype but not mutant DCDC2 localize to the primary cilia in RPE1-cells.

RPE1 cells transfected with wildtype human DCDC2 show localization to the primary cilium. The localization is abrogated in all mutations found in humans with ciliopathies (rows 2-4) and in artificial constructs, in which either of the two doublecortin domains are missing (rows 5 and 7). DNA was labeled with DRAQ5 (blue). Scale bar 10µm.

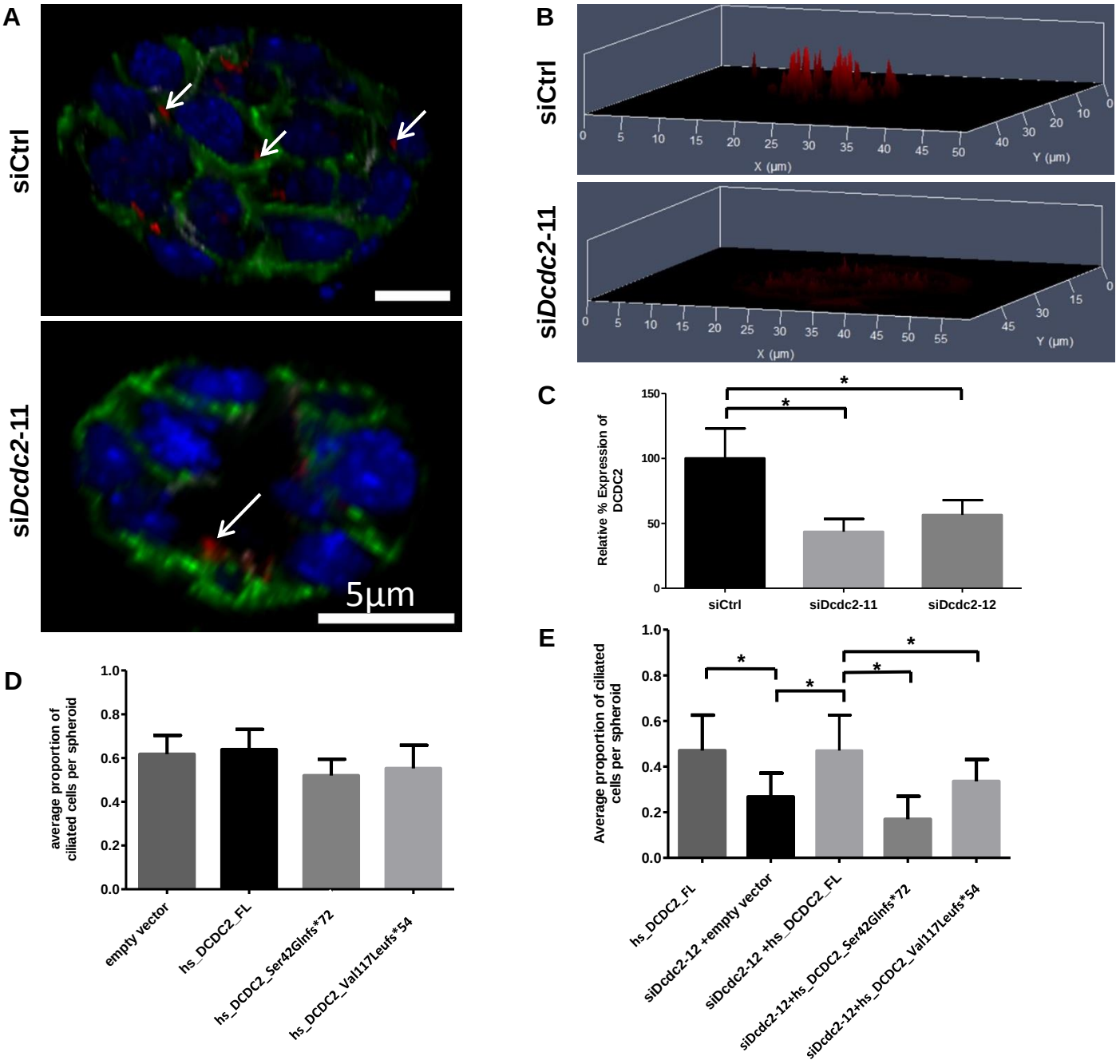

Figure S10. 3D representation of cilia loss after *Dcdc2* knockdown in IMCD3 cells.

*Dcdc*2 knockdown causes a ciliation defect, which is not rescued by *DCDC2* mutants detected in NPHP-RC, but is rescued by overexpression of full length human *DCDC2* (hsDCDC2_FL).

(A) 3D renderings of partial Z-stacks of IMCD3 spheroids show a loss of ciliation after *Dcdc2* knockdown (settings are identical between conditions). Acetylated tubulin (red, marked with arrows) indicates the presence of cilia.

(B) 2.5D surface renderings of Z-stacks demonstrate that the intensity of acetylated tubulin staining in the lumen of spheroids noticeably decreases after *Dcdc2* knockdown.

(C) qPCR validation of the knockdown efficiency of siRNA *DCDC2*-11 *and DCDC2*-12 in IMCD3 cells.

(D) Average proportion of ciliated IMCD3 cells per spheroid for overexpression of full length human *DCDC2,* empty vector, and three mutants found in humans with ciliopathies, showing no effect on ciliary frequency.

(E) Average proportion of ciliated IMCD3 cells per spheroid upon knockdown with a second siRNA (si*Dcdc2*-12A) as validation of the observed ciliogenesis defect and allelic reconstitution.

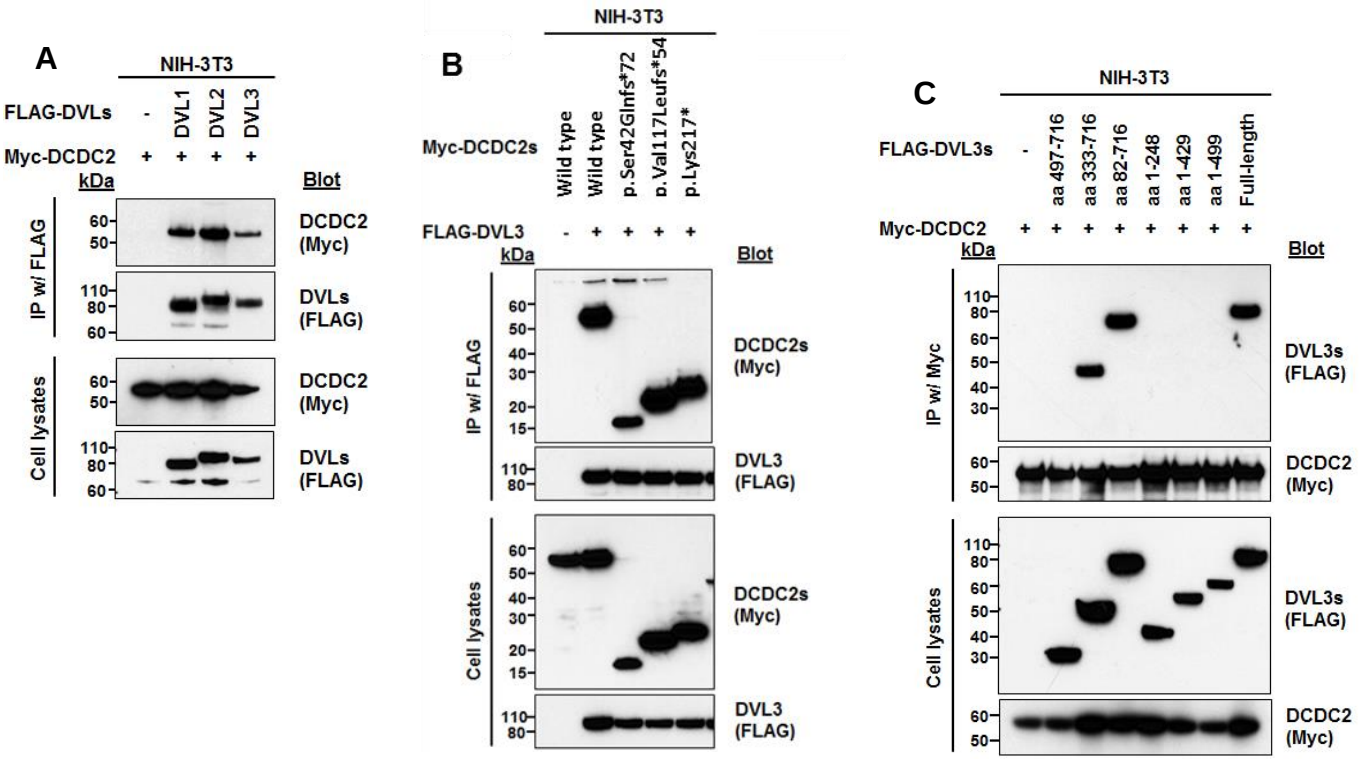

Fig S11. DCDC2 interacts with dishevelled (DVL). The human mutations do not abrogate the interaction.

(A) Co-immunoprecipitation with Myc tagged DCDC2 and Flag tagged Dvl shows that DCDC2 interacts with DVLs (DVL1, DVL2 and DVL3) when transiently overexpressed in NIH-3T3 cells.

(B) None of the three human mutations abrogate this interaction.

(C) The partial DVL3 clone (497-716aa) and the C-terminal DVL3 deletion clones (1-248 aa, 1-429 aa and 1-499 clones) show loss of interaction with DCDC2 by immunoprecipitation using a Myc-tag of DCDC2. Therefore, the C-terminus of DVL3, which includes a DEP (Dishevelled, Egl-10 and Pleckstrin) domain, is necessary for the interaction with DCDC2.

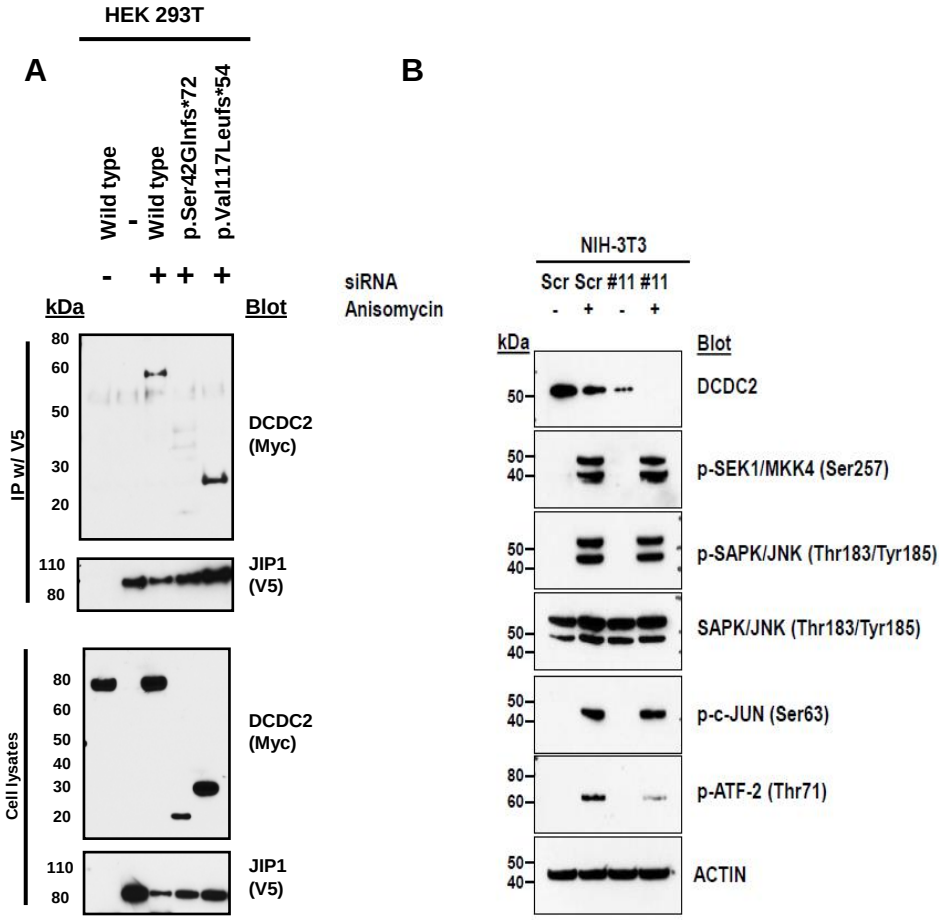

Figure S12. DCDC2 interacts with JIP1.

(**A**) Protein-protein interaction between DCDC2 wild-type (WT) and JIP1 full length (lane 3), and the effect of the two *DCDC2* mutations p.Ser42Glnfs*72 and p.Val117Leufs*54 on the interaction with JIP1 (lanes 4 and 5). Note that while p.Val117Leufs*54 still interacts with JIP1 (lane 5), p.Ser42Glnfs*72 abrogates the interaction between DCDC2 and JIP1 (lane 4). (For DCDC2 constructs see **Suppl. Fig. 2**)

(**B**) Knockdown (#11) of *Dcdc2* in NIH-3T3 cells does not affect the JNK pathway activation. Scrambled (Scr) siRNA was used for negative control. Phosphorylation of the JNK downstream target c-Jun and ATF2 was used as the read-out. Anisomycin (50 μg/ml) shows pharmacological activation of the pathway and increased phosphorylation of c-Jun and ATF2.

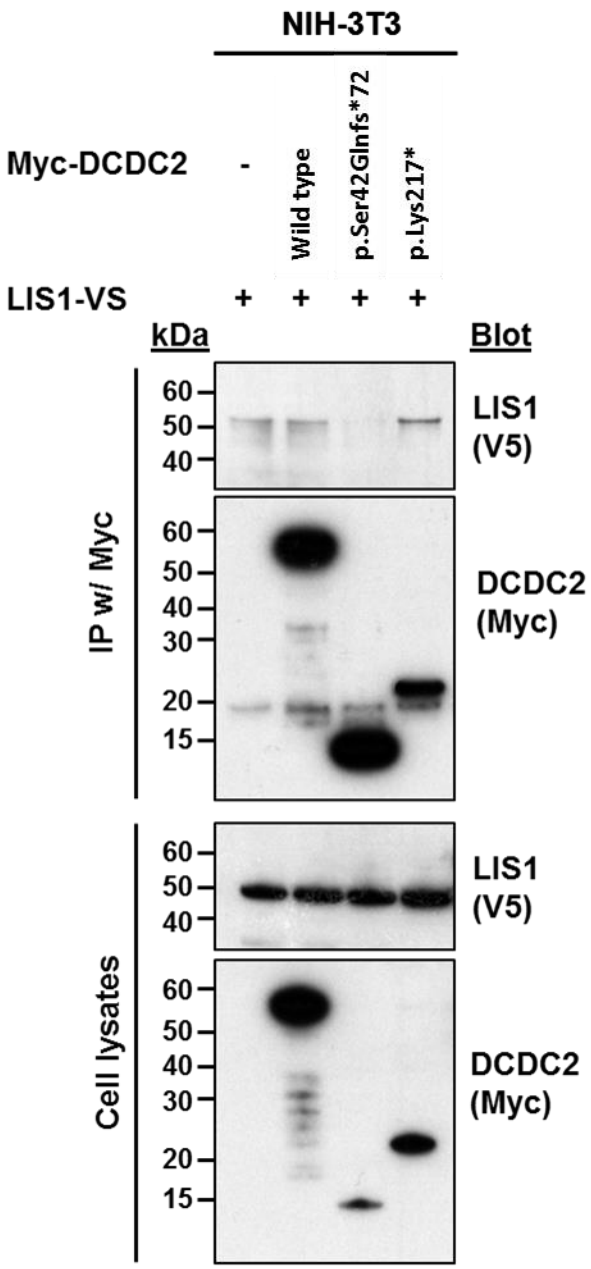

Figure S13. DCDC2 does not interact with LIS1.
C-terminally V5-tagged *LIS1* and N-terminally Myc-tagged *DCDC2* constructs were transfected into NIH-3T3 cells and coimmunoprecipitated with a Myc antibody. There was no protein-protein interaction between LIS1 and DCDC2. Images are representative of two experiments. IP denotes immunoprecipitaiton.

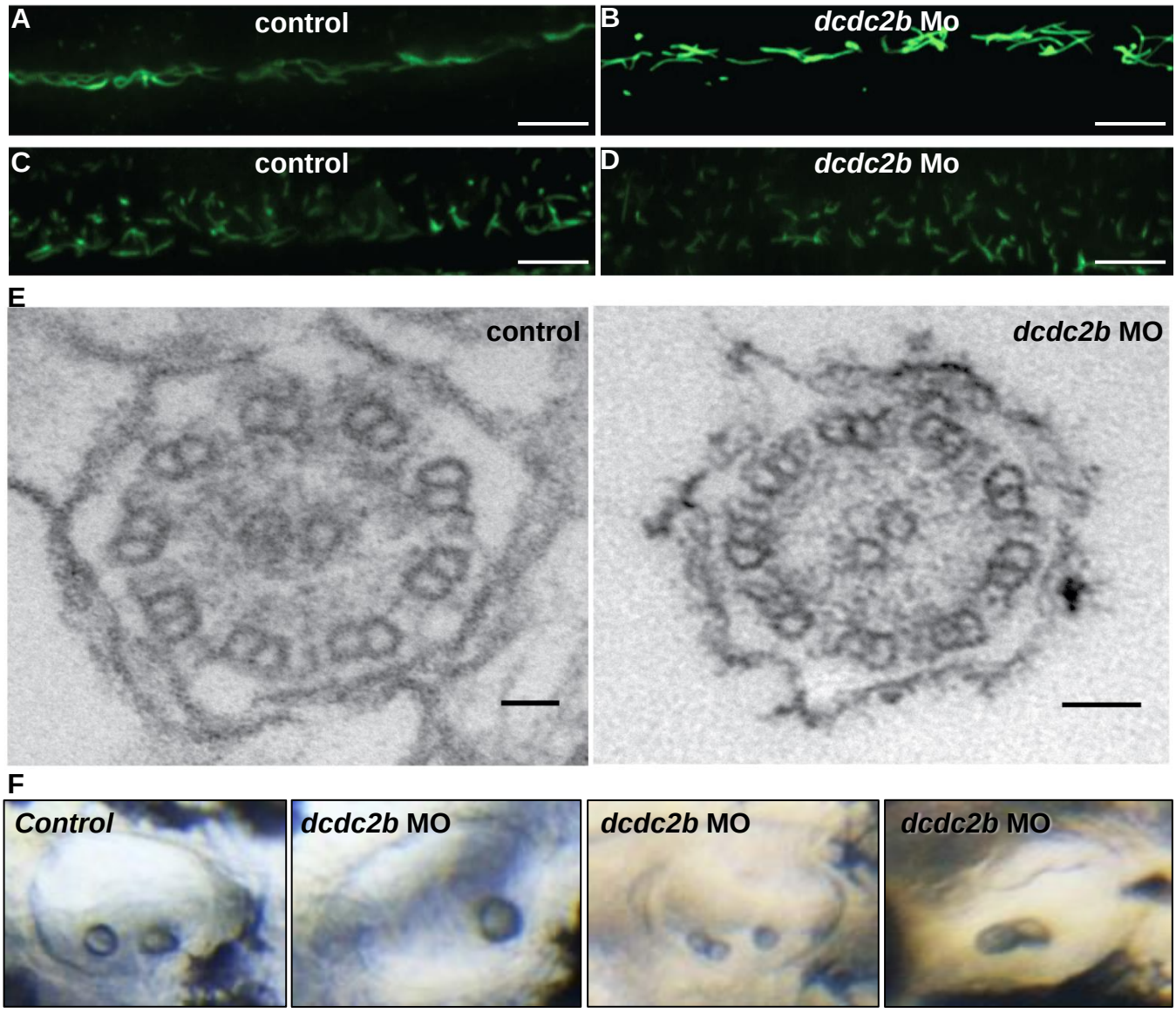

Figure S14. Knockdown of *dcdc2b* does not alter cilia length in zebrafish kidney and spinal cord nor ultrastructure of pronephric cilia.

Pronephric cilia of control and of *dcdc2b* morphant zebrafish embryos were immunostained one day post fertilization with anti-acetylated α-tubulin antibody**.**

(A/B) Cilia (green) in pronephric kidney of *dcdc2b* MO (right panel) do not show a difference in length compared to uninjected control (right panel).

(C/D) Spinal cord cilia length did not differ in length between conditions of control(left panel) and MO knockdown (right panel). Scale bar: 50 um

(E) The ultrastructure of motile cilia in pronephric kidney does not differ between conditions of control (left panel, scale bar: 200 nm) and *dcdc2b* MO knockdown (right panel, scale bar 100 nm).

(F) Representative images of *dcdc2b* morphants (AUGMo) at 3 dpf show variable otolith numbers ranging from 1-3 (64/147 = 43.5%), whereas control display normal pattern of two otoliths (5/114 = 4.4%).

Table S1. Filtering process for variants from normal reference sequence (VRS) following WES in one sibling from family A3547-22 affected with NPHP-RC.

FAMILY	A3547
[a]AFFECTED individual SENT FOR WES	A3547-22
Consanguinity	Yes
[b]# of homozygosity peaks	8
Cumulative Homozygosity by descent[c] [Mb]	124
[c]Hypothesis from mapping: homozygous (H), heterozygous (h)	H
Total sequence reads (Mill.)	454
Matched Reads	98.1%
Total DIPs	10,259
Exonic DIPs	249
% exonic / total DIPs	2.40%
DIPs in linked region	16
DIPs after inspection and not SNP138 (>1% MAF)	0
Sanger confirmation / Segregation	0
Total SNPs	29,402
Exonic SNPs	1,674
% exonic / total SNPs	5.60%
SNPs in linked region	139
SNPs after inspection and not SNP138 (>1% MAF)	5
[d]Sanger confirmation / Segregation	1
gene with causative mutation	*DCDC2*
Mutation effect on gene product	K217* (H)

[a]see Table 1

[b]see Fig. 1

[c]evaluation for homozygous variants was done in regions of homozygosity by descent for 1 affected individual

[d]red numbers denote number of filtered-down variant(s) that contained the gene with disease causing mutation

DIP, deletion/insertion polymorphism; SNPs, single nucleotide polymorphism; NPHP-RC, Nephronophthisis-related ciliopathies

Table S2. Final remaining variants after filtering process

DCDC2 truncating mutation is highlighted in yellow to indicate ranking as most likely disease causing.

Diagnosis: NPHP-RC

Total homozyg. [Mb]: 124041201
Hom. peaks: 8
Other captures: No

Poly 2
0 - 0.7
0.7 - 0.9
0.9 - 1.0

individual	Gene	hg19 pos.	Nt change >	Accession #	AA change p.	Conservation							Mut Taster	SIFT	Poly2	EVS
						Mm	Gg	Xt	Dr	Ci	Ce	Dm				
A3547-22	*DCDC2*	chr6:24291215	T>A	NM_001195610.1	p.K217*											no
	TATDN3	chr1:212981117	C>T	NM_001042552.2	p.P176L	P	P	P	P	S	P	A	Pol	Del	0.015	no
	BIRC6	chr2:32667182	G>C	NM_016252.3	p.V1332L	L	L	T	L	S	-	-	DC	Del	0.9	no
	CCDC66	chr3:56650056	>CTC	NM_001141947.1	p.S606delinsSP	S	-	-	Q	-	-	-				A1A1=76/A1R=525/RR=1201
	CLDN16	chr3:190106073	G>C	NM_006580.3	p.R55S	Q	-	-	-				Pol	Tol	0.01	no

Table S3: Primer

Primer	Primer Sequence Forward	Primer Sequence Reverse	Size
DCDC2, Exon2_1	CGAAGCTGGACACCTTCTT	CTCTTTCACCTGTGGATTCG	271bp
DCDC2, Exon 2_2	ATCTGCATTTCTTCATATCAACC	CCTTCTACGCGGGGC	287bp
DCDC2, Exon3	GAGAACTCATCAAAGTAGAATGCC	AACTCTTATTGTTTGTTTGTTTTTTCC	188bp
DCDC2, Exon4	GCAAGGTTTTAACAAAGGCAC	CAAACCAAAAGGAAACCACC	262bp
DCDC2, Exon5	TCAACAATTCAAAAACTCCTCC	TGGTTTCCTTTTGGTTTGG	257bp
DCDC2, Exon6_1	TGGTGGTCAGCAAAAGACC	GAAGGAAAACTTGTTGAGAGTGG	209bp
DCDC2, Exon6_2	GCAGTTTCTTAAACTTATCTCTGCC	GGCATCTATAATGCAATAATGAGG	270bp
DCDC2, Exon 7	ACAGTTGACTTCCAGGTGGG	GAAGCCCAAAGGACAGTCTC	222bp
DCDC2, Exon8_1	GGCCCAGAGAAACAATGG	GGTCTAATACTTTGCCATTTAGGG	259bp
DCDC2, Exon8_2	AATTCACGTCTTCTTTTTTCCC	ACCCTTTTGCCTCCAGG	275bp
DCDC2, Exon9	CCTTAGAGGGTTTAATTCATACAGG	CAGCATTCAGCCACACG	278bp
DCDC2, Exon10_1	CATTCACATAAGCAAGCAAAAGC	TGACCTTGAAGAGGAAGGAGG	248bp
DCDC2, Exon 10_2	CTCACCATTCTCCTCATC	GCAGTGGAAATGTTCTGTTATGC	279bp
DCDC2, Exon11	TGCTTATCTTTCAAGTATGATAACCC	TTACCTTTGTGAACCAAACAGC	229bp
DCDC2, cDNA exon2	CGGAAGCTAGACCAGATCCA		
DCDC2, cDNA exon5		CCGCTCCTCAGAGTGATTTT	
Dcdc2b ATG MO	CCGGTGGATGCCATGACTTTTCAGT		
Dcdc2b Splice MO	GCCATGACCTTAAATTAATCACATT		
siRNA murine dcdc2	CCAGAUGCCUAAAGCGUUA		
siRNA murine dcdc2	GAUGCAGGGCAGCGCUUUA		